DECEMBER 1981

HEWLETT-PACKARD JOURNAL

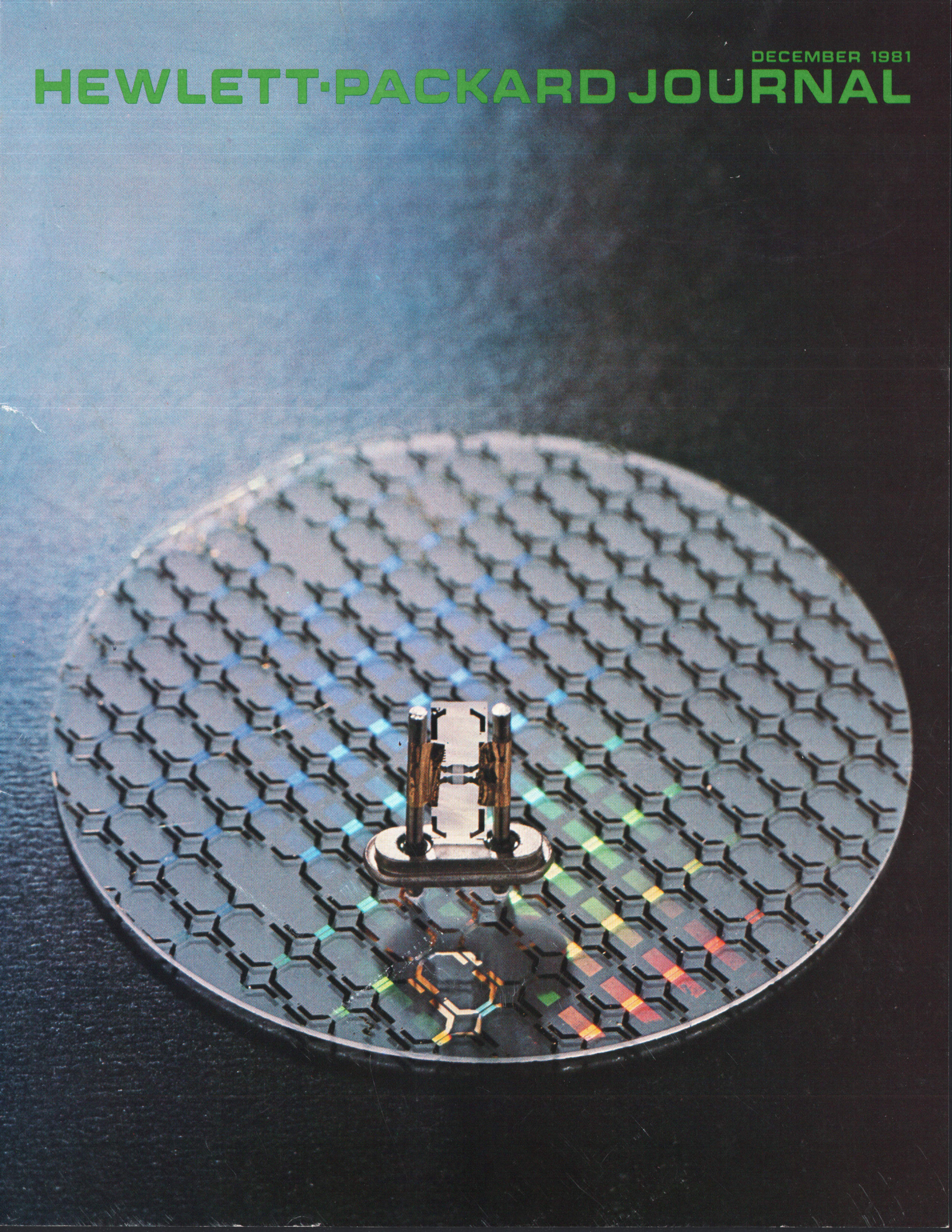

HEWLETT-PACKARD JOURNAL
Technical Information from the Laboratories of Hewlett-Packard Company

DECEMBER 1981 Volume 32 • Number 12

Contents:

In this Issue:

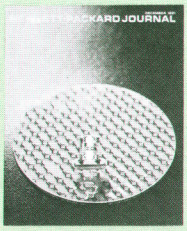

Most of this issue is about SAWs—not the cutting kind, with teeth, but *surface acoustic waves*. These are like the waves or ripples that radiate outwards from the spot where a pebble is dropped into a pond. Instead of water, the surface acoustic waves described in this issue propagate on the surface of a solid, such as a piece of quartz. Of course, the atoms in the solid don't move as much as the water molecules do; one can't even see these SAWs. But it turns out that by guiding and controlling these waves, it's possible to create electronic components that perform useful functions and have advantages over other ways of performing the same functions. SAW devices include delay lines, filters, resonators, sensors for temperature, pressure, force, or displacement, and various exotic processing devices such as correlators and convolvers. The waves are called acoustic not because you can hear them but because they are vibrational rather than electromagnetic waves. Their operating frequencies are by no means limited to audible frequencies. Some SAW devices operate in the gigahertz range and find applications in sophisticated radar systems.

The articles in this issue represent both an introduction to SAW devices and a discussion of the work being done on them at Hewlett-Packard. Delay lines and filters are described in the article on page 3, resonators on page 9 and sensors on page 18. The article on page 11 discusses how SAW resonators are made (many integrated circuit processing techniques are used) and the article on page 15 tells about the first SAW device used in an HP instrument, a 280-megahertz SAW resonator (pictured on this month's cover) that replaces a quartz crystal resonator in the 8558B and 8568A Spectrum Analyzers. Associate editor Ken Shaw had a good time editing these articles because he wrote his doctoral thesis many years ago on SAW devices. He's working on another article on SAW signal processing for an upcoming issue.

Among the integrated circuit techniques sometimes used in making SAWs is electron beam lithography. Our May 1981 issue was all about this technology and HP's high-speed electron beam lithography system. A fact of life in electron beam lithography is that electrons scatter when they hit a solid target, so when you try to expose very fine lines (less than a micrometre wide) very close together on a layer of electron-sensitive material, the contour of a given line may be affected by the presence of nearby lines. This is called proximity effect. On pages 21 and 24, four Hewlett-Packard scientists report on research into methods of controlling this effect.

December is our annual index issue. You'll find this year's index on pages 28-32.

-R.P. Dolan

Surface-Acoustic-Wave Delay Lines and Transversal Filters

Novel, simple and compact electronic devices can be realized by exciting and detecting acoustic waves electrically on the surface of a solid. Technological advances in low-loss delay lines and bandpass filters are discussed.

by Waguih S. Ishak, H. Edward Karrer and William R. Shreve

SURFACE WAVES are familiar to anyone who has thrown a pebble into a pond and watched the concentric ripples emanate from the splash. These waves carry energy outward from the splash at a velocity dependent on the properties of the medium and the magnitude of the restoring force, in this case water and gravity. An observant person on the shore would notice that a cork floating on the surface would follow an elliptical path in a vertical plane as the wave passed (Fig. 1a). An observer, perhaps a fish, at the bottom of a deep pond would not feel these waves since they are confined to a surface layer about one wavelength thick.

Surface waves also can exist on solids. These waves were first analyzed by Lord Rayleigh in 1885.[1] His work explained one of the classic problems of geology in the last century, that is, how to locate an earthquake by interpreting seismogram recordings from several locations. Rayleigh showed that an earthquake not only generates longitudinal (compressional) and transverse (shear) waves which tend to follow chordal paths through the earth, but also surface waves which travel at a slower velocity around the earth's circumference. The surface waves are guided by the stress-free boundary between the earth and its atmosphere. These waves cause the largest ground motion in an earthquake.

During this century, surface waves were extensively studied by the Russian scientist Viktorov.[2] He showed that surface waves on a solid have a surface particle motion that is retrograde elliptical and opposite to the motion of a particle caused by a surface wave on water (Fig. 1). He also showed that the amount of particle motion falls off exponentially with depth below the surface.

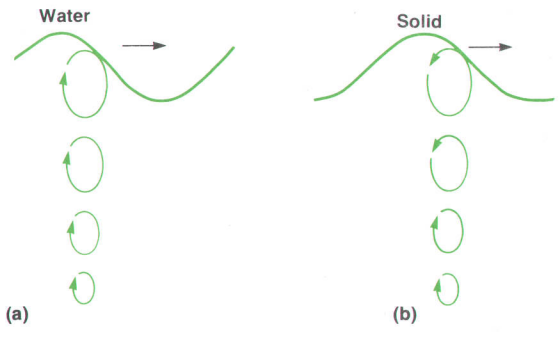

Fig. 1. *The amplitude of the motion of particles in a medium disturbed by the passage of a surface wave decreases with the depth of the particle below the surface. In a liquid (a) the motion at the surface is in the opposite direction from motion in a solid (b).*

A real breakthrough came in 1965 when White and Voltmer discovered an easy way to generate and detect surface acoustic waves (hereafter abbreviated SAWs) in the laboratory.[3] They used metallic interdigital transducers (IDTs) deposited in a vacuum on a piezoelectric substrate (Fig. 2). In an IDT the fingers are spaced by $\lambda/2$ where $\lambda = v/f$. Here f is the excitation frequency, v is the surface wave velocity, and λ is the wavelength.

When an alternating voltage of frequency f is applied to the IDT, an electric field is created between adjacent fingers. A strain field is also generated because of the electromechanical interaction in the piezoelectric substrate. This strain field is an imprint of the IDT and propagates away from the IDT in both directions as a surface wave. The surface wave can be detected by a second remote IDT as the SAW passes through it because the surface wave carries with it an electric field via the piezoelectric effect which generates a voltage between adjacent IDT fingers.

This advance in SAW excitation initiated a new wave of interest in SAW devices to capitalize on their novel properties. Such devices are small because surface-wave velocities are typically 3000 metres per second, five orders of magnitude slower than electromagnetic waves. The IDT is a planar structure that can be made with a single metallization step. Advances in microelectronic fabrication and photolithography brought about by the booming semiconductor industry were immediately applicable to the emerging SAW technology. The growing research led to new piezoelectric materials and material cuts optimized for particular requirements such as temperature stability or large fractional bandwidth.

The advance of SAW technology can be traced in more detail by the interested reader who examines some review articles, special issues of technical publications, and books published in the field.[4-9]

Delay-Line Filters

Delay-line filters were among the first SAW components to be used in circuits. The impulse response of these filters can be accurately controlled in both amplitude and phase, and their nondispersive nature leads to a linear change of

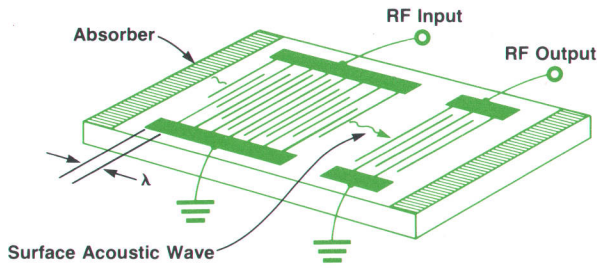

(a)

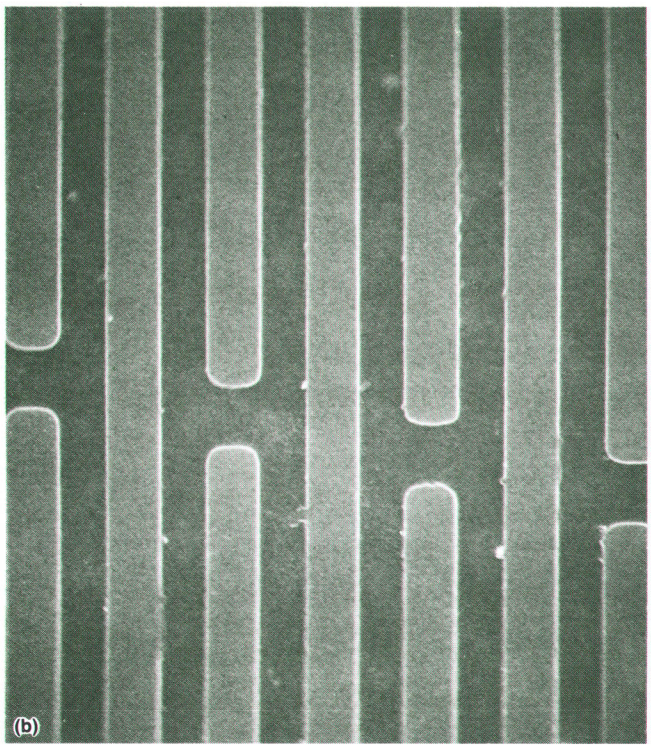

Fig. 2. *(a) Basic configuration for a surface-acoustic-wave delay line. The absorbing layer at each end reduces reflections from the edges of the substrate. (b) Scanning electron microscope photograph of a section of a typical interdigital transducer at 2300×. The varying lengths (apodization) of the electrodes are chosen for a desired response.*

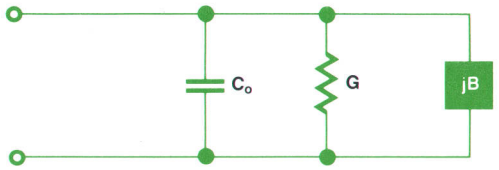

Fig. 3. *Equivalent circuit for an interdigital surface-acoustic-wave transducer (IDT).*

phase with frequency. It is even possible to distort the filter's phase response intentionally to compensate for phase shifts in matching networks or other circuit components.

The key element in SAW filter design is the interdigital transducer; it couples the electrical signal to the acoustic waveform and thereby determines the filter impedance and frequency response. The transducer can be modeled by the equivalent circuit in Fig. 3. For a transducer consisting of N pairs of electrodes N_A wavelengths long, these circuit elements are

$$C_o = NN_A\lambda_t\,(\epsilon_p+\epsilon_o)$$
$$G = G_o\,[\sin(x)/x]^2$$
$$B = G_o\,[\sin(2x)-2x]/(2x^2)$$
$$G_o = 8k^2\,v_t\,(\epsilon_p+\epsilon_o)N^2N_A$$
$$x = \pi(f-f_t)N/f_t$$

where λ_t is the wavelength at the transducer's center frequency f_t, ϵ_p is the effective dielectric constant of the substrate, ϵ_o is that of air, k^2 is the piezoelectric coupling coefficient of the substrate, f is the frequency and v_t is the acoustic velocity under the transducer (the effects of mechanical reflections from the transducer electrodes are neglected in these expressions). Note that the transducer conductance G is not constant with frequency. This variation largely determines the filter frequency response. If the lengths of the electrodes are varied (a technique called transducer apodization, see Fig. 2b), the frequency response can be tailored to a given application.

Initially, the use of SAW devices to provide filtering was limited by the properties of the conventional interdigital transducer. The transducer is inherently a three-port device

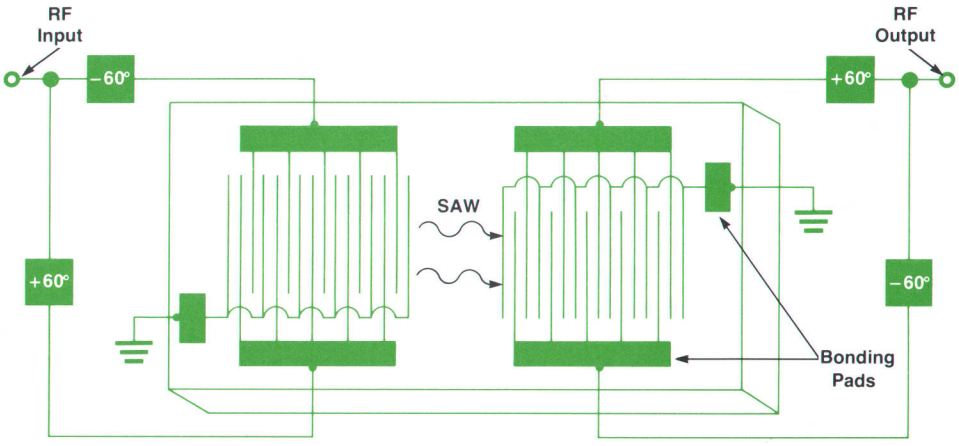

Fig. 4. *Configuration for a SAW delay line using three-phase unidirectional IDTs. Multilayer metallization is required because some conductors must pass over other conductors in this design.*

with one electrical port and two acoustic ports. In the conventional filter arrangement (Fig. 2) the power is divided by the launching transducer. Half is sent toward an absorber and half propagates toward the output. At the output transducer, some of the signal (at most half) is delivered to the load, some passes the transducer and is absorbed, and some is reflected. Thus the minimum loss, 6 dB, is achieved when the electrical ports are perfectly matched.

Unfortunately, this matching condition also maximizes the reflection from the transducer. When the signal reflected by the output IDT reaches the input IDT part of it is reflected back to the output. The doubly reflected signal is detected at the output and causes passband ripple. This triple-transit signal can only be reduced by mismatching the transducer. For a delay line with identical transducers, this can be expressed simply in terms of the normalized conductance $g=GZ_L$ where Z_L is the load impedance. The ratio of the single-transit signal amplitude to the input signal amplitude is

$$\frac{\text{single-transit}}{\text{input}} = \frac{2g}{(1+g)^2}$$

and the ratio of the triple-transit signal to the input is

$$\frac{\text{triple-transit}}{\text{input}} = \frac{2g^3}{(1+g)^4}$$

When the transducer is matched ($g \Rightarrow 1$), the triple-transit signal amplitude approaches one-quarter of the single-transit signal amplitude. This corresponds to 4 dB of ripple on a nominal 6-dB-loss filter.

One solution to this problem of having either high insertion loss or significant ripple is to use unidirectional transducers to couple all of the electrical energy into a single acoustic wave. This eliminates one acoustic port and thereby reduces the ideal minimum loss to 0 dB. Since there are only two ports, the SAW delay line can be perfectly matched and reflections can be eliminated. Unidirectional transducers are made with phased arrays of electrodes, usually three or four electrodes per wavelength as shown in Fig. 4. This design complicates the fabrication process by introducing multiple layers of metallization and complicates the electrical matching by requiring multiphase excitation voltages. However, most integrated circuits also require multilayer metallization so the SAW fabrication problem is not severe. On the other hand, the matching requirements limit filter bandwidth and increase the component count. Three or four reactive elements are required at each end of the three-phase transducer in Fig. 4.

Another design achieving unidirectional operation uses pairs of bidirectional transducers spaced by one-quarter wavelength and driven 90 degrees out of phase. The waves from the pairs add in one direction and cancel in the other. Sets of these pairs can be combined to give the desired frequency response. As shown in Fig. 5, multilayer metallization can be eliminated by running the ground electrode between the groups. In general, two components are required to generate the phase shift and match this transducer. However, in practice a single inductor can be used. The major drawbacks of this type of unidirectional transducer are the extra loss introduced by the meandering ground and the presence of extra passbands introduced by the periodicity of the groups.

SAW filters can give more rapid rolloff from passband to sidelobe floor than any other type of UHF* filter. There are a number of techniques to give the desired shape factor (the ratio of 40-dB bandwidth to 3-dB bandwidth), bandwidth, and sidelobe level with minimum insertion loss and complexity, but these specifications are linked. Small shape factors and low sidelobes require long transducers that increase substrate size and progagation loss. Filter bandwidth is limited by the acoustic Q as set by the crystal's piezoelectric coupling coefficient. On ST-cut α-quartz, the material used for stable operation over temperature, the maximum fractional bandwidth that can be achieved without additional loss is about 3%. On a stronger coupling material like $LiNbO_3$ (lithium niobate) the limit is about 20%, but matching unidirectional transducers over a bandwidth of more than 5% can be difficult.

SAW filters have unique capabilities and will be found in an increasing number of military and commercial systems. When designing SAW devices into circuits, it is prudent not to overstate one's requirements since a particularly stringent requirement may force compromises in other

*Ultrahigh frequency, the range from 300 MHz to 3000 MHz.

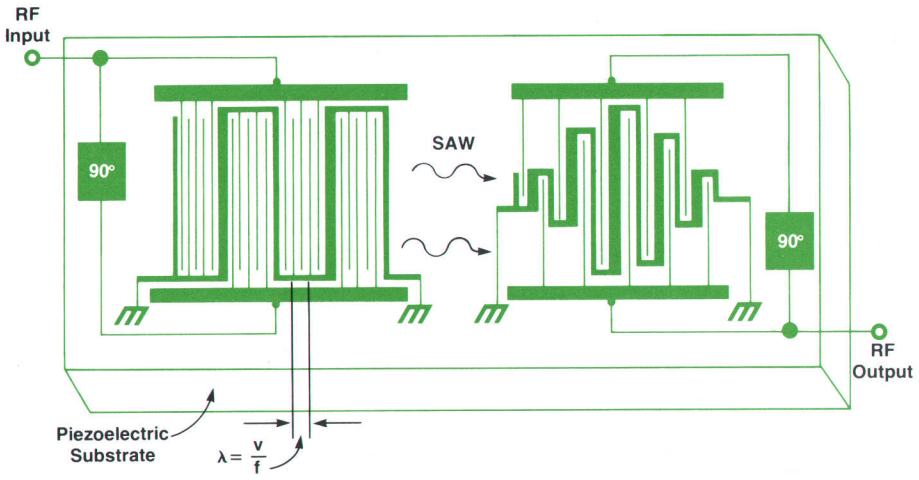

Fig. 5. *Configuration for a SAW delay line using group-type unidirectional IDTs. This design eliminates the need for multilayer metallization by using a meandering ground electrode pattern as shown.*

specifications. For example, fractional bandwidths exceeding about 5% lead to insertion loss above 7 dB or passband ripple exceeding 1 dB. Sidelobe levels more than 40 dB below the passband and shape factors less than 2:1 lead to higher insertion loss and a maximum bandwidth of a few percent. Therefore, filter specifications for particular applications should be considered carefully in light of the tradeoffs that exist.

Bandpass Filter Design

SAW bandpass filters with a fractional bandwidth of less than 5% can be accurately synthesized using a delta-function model. Each gap between electrodes of different phases is modeled by an impulse whose amplitude is proportional to the electrodes' active overlap at the gap. A computer program has been written to model both bidirectional and unidirectional SAW IDTs. The program runs on an HP 1000 Computer and has been tested extensively for various filter configurations.

Inputs to the program are center frequency, bandwidth and apodization functions. A library of apodization functions is included to achieve various frequency responses. The program represents the impulse response at each gap location by a delta function and then computes the Fourier transform to get the frequency response. The user can iterate the input parameters to achieve the desired frequency characteristics for each transducer and then, upon command, the program calculates and plots the combined filter response in the desired format.

To verify the design concepts embodied in the program, an experimental SAW filter was built at Hewlett-Packard Laboratories. The filter consisted of two conventional bidirectional transducers with a center frequency of 321 MHz. The synthesis program generated the optimum transducer configuration and the filter was fabricated on a 2.5-mm-square substrate of Y-cut, Z-propagating $LiNbO_3$. Fig. 6 shows the frequency response of such a filter which is in fair agreement with the model. Table I compares the design parameters with the actual values. The combination of high insertion loss (>10dB) and ripples (>1dB) necessitated using another scheme for the IDTs.

As discussed earlier, several methods exist for realizing unidirectional IDTs. Group-type unidirectional transducers (GUDTs) like those in Fig. 5 were chosen for several reasons.[10] First, they require only one layer of metallization

Table I
Comparison of Theoretical and Actual Parameters for 321-MHz SAW Filter

Parameter	Design Value	Actual Value
Center frequency (MHz)	321.4	321.4
Insertion loss (dB)	<10	11.0 (matched) 14.2 (unmatched)
3-dB bandwidth (MHz)	>10	18
Ripples (dB)	<0.5	1.2 (matched) 0.8 (unmatched)

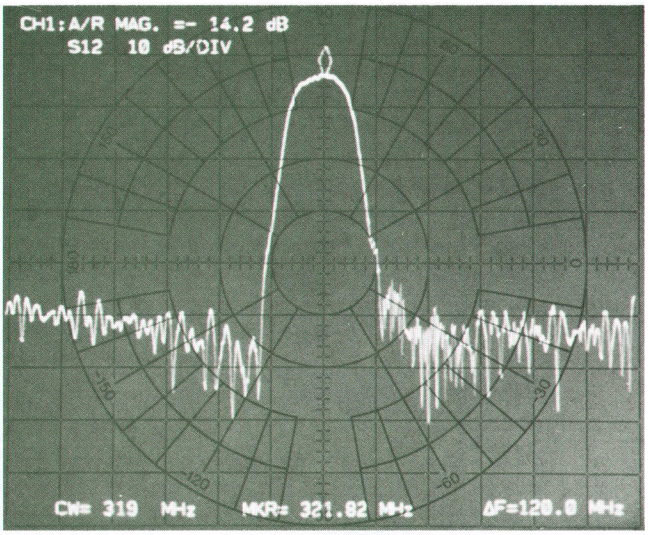

Fig. 6. *Frequency response of a 321-MHz SAW filter using bidirectional IDTs. The design was generated by a computer program developed at HP Laboratories.*

which makes fabrication easy. Second, the minimum dimension is one-quarter wavelength, allowing frequencies up to 1 GHz on $LiNbO_3$ before the dimensions become fine enough to make fabrication difficult. Third, matching and phase shifting networks are much simpler than those required for three-phase unidirectional transducers.

The design program was modified to model GUDTs. The modified program yields the matching network and the optimum transducer aperture (length of the finger electrodes) to achieve both matching and unidirectionality. This is done by using the equivalent circuit shown in Fig. 3 for each phase and requiring that the transducer input impedance be equal to the source impedance and that equal power (with 90° phase shift) be delivered to each phase. The program was tested and proved to be accurate in predicting the frequency response of GUDT filters.[11]

To test the accuracy of the model, several filters were built with identical transducers. The agreement between the predicted and measured frequency responses was good as demonstrated by the results for a 650-MHz filter in Fig. 7. These results also illustrate the characteristic multiple passband response of GUDTs caused by the periodicity of the groups.

In practical filters, the sizes of the groups in the two transducers are not the same. The extra passbands of one transducer align with minima in the second transducer's response. Thus, the extra bands are suppressed in the composite filter response. Matching the transducers with inductors further reduces these spurious responses. In most cases, the extra bands are at least 35 dB below the main passband level.

The output of the design program is fed into another program to generate the final pattern generator tape for production of the photomask. In this program, the electrode positions are combined with bonding-pad locations to define the entire filter chip. After receiving and inspecting the completed mask, the filters are fabricated using the procedure described in the box on page 11 except that no

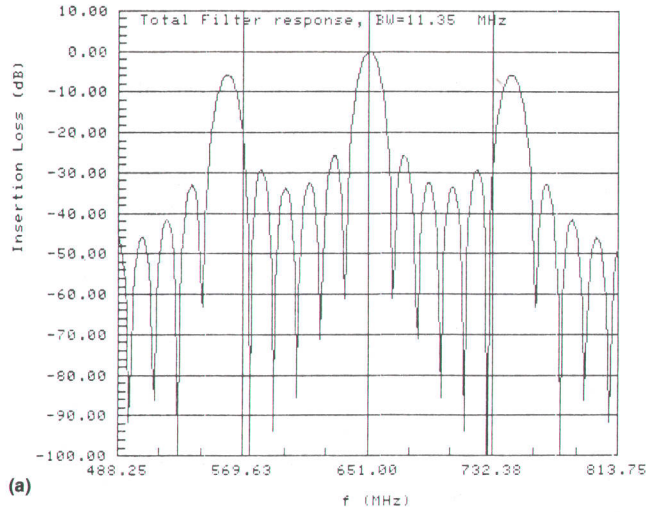

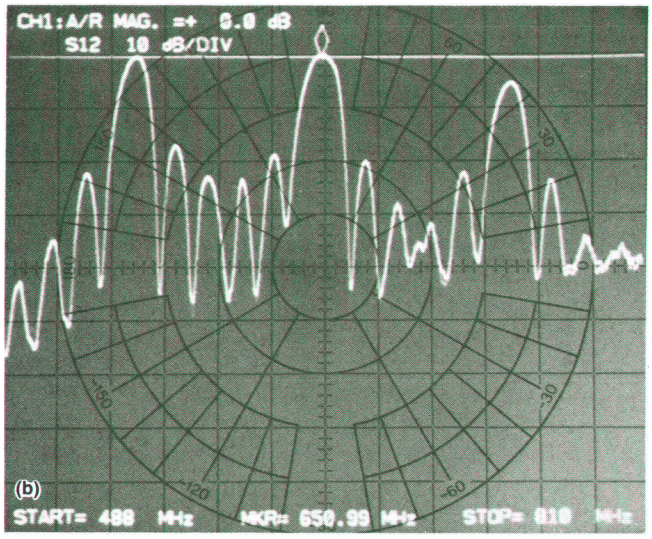

Fig. 7. *Frequency response of a 650-MHz GUDT filter with identical transducers. Note the extra passbands caused by the group periodicity. (a) Model prediction. (b) Experimental result.*

reactive-ion-etching step is required. These devices are then tested using an HP Model 8507A Network Analyzer.

Experimental Results

Several designs for GUDT filters at frequencies ranging from 300 to 750 MHz have been studied. The piezoelectric material used for its high electromechanical coupling factor was 128° rotated Y-cut, X-propagating $LiNbO_3$. The frequency response of one of these filters is shown in Fig. 8. The matching and 90° phase shift for each transducer were obtained with a single 4-turn airwound 2-mm-diameter coil. The figure shows the agreement between the model and experiment over an octave bandwidth, the degree of suppression of the extra bands achieved from a careful choice of transducer groups, and the sidelobe suppression caused by the matching coils. The filter insertion loss is 5.4 dB at the center frequency of 364 MHz, and the out-of-band rejection is better than 40 dB.

In Fig. 8c the response is shown using expanded scales

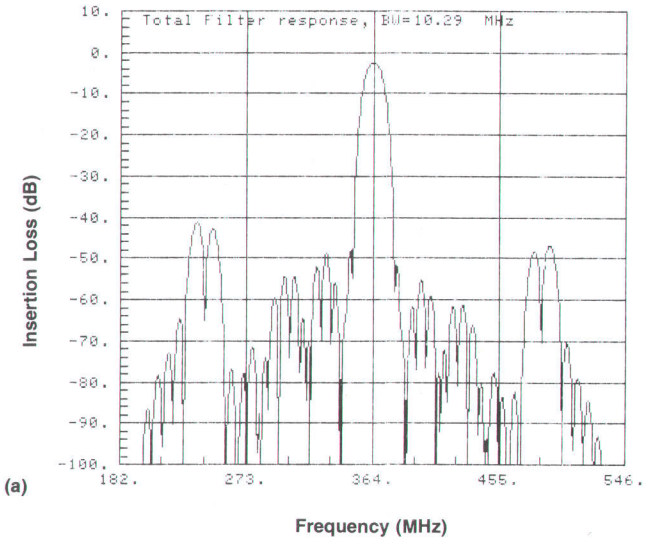

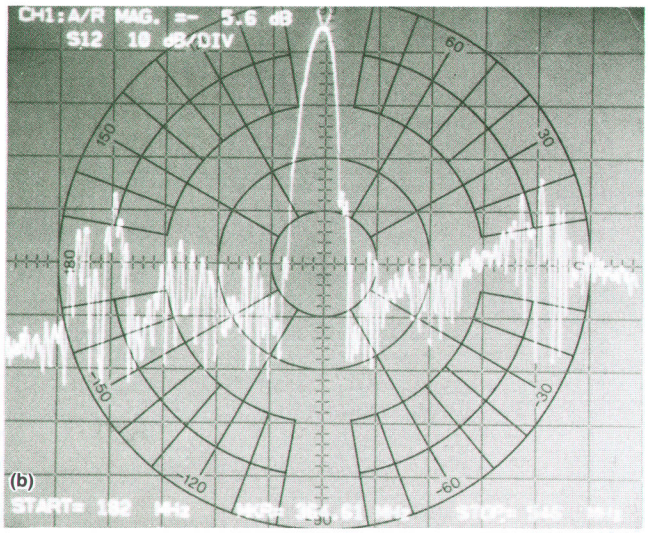

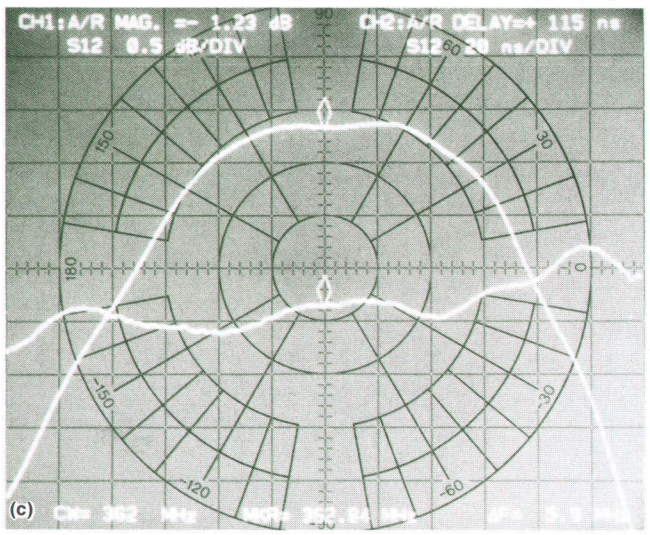

Fig. 8. *Frequency response of a typical GUDT SAW bandpass filter. Insertion loss is 5.4 dB. (a) Model prediction. (b) Experimental result. (c) Expanded display of the filter response shown in (b). The bandwidth is 10.8 MHz and the ripples in the group delay are less than 20 ns.*

(0.1 dB) to indicate how flat the response is. The passband ripples are smaller than 0.01 dB. Also, we notice that ripples in the group delay are less than 20 ns over the entire 10.8-MHz bandwidth of the filter.

Acknowledgments

Many people have contributed to the success of the SAW program at Hewlett-Packard. We would particularly like to thank Charles A. Adams and John A. Kusters for their pioneering work to establish SAW technology here and Johnny Ratcliff and George Nelson for their technical support.

References:

1. Lord Rayleigh, "On Waves Propagated Along the Plane Surface of an Elastic Solid," Proceedings of the London Mathemetical Society, Vol. 17, 1885, pp. 4-11.
2. I. Viktorov, "Rayleigh and Lamb Waves," Plenum Press, New York, 1967.
3. R.M. White and F.W. Voltmer, "Direct Piezoelectric Coupling to Surface Elastic Waves," Applied Physics Letters, Vol. 7, December 1965, pp. 314-316.
4. Special issue on microwave acoustics, IEEE Transactions on Microwave Theory & Techniques, Vol. MTT-17, November 1969.
5. Special issue on microwave acoustic signal processing, IEEE Transactions on Sonics & Ultrasonics, Vol. SU-20, April 1973.
6. Special issue on surface acoustic waves, Proceedings of the IEEE, Vol. 64, May 1976.
7. H. Matthews, "Surface Wave Filters," John Wiley and Sons, New York, 1977.
8. A. A. Oliner, "Acoustic Surface Waves," Springer-Verlag, New York, 1978.
9. Special issue on SAW device applications, IEEE Transactions on Sonics & Ultrasonics, Vol. SU-28, May 1981.
10. K. Yamanouchi, J. Nyffeler and K. Shibayama, "Low Insertion Loss Acoustic Surface Wave Filters Using Group-Type Unidirectional Transducers," IEEE Ultrasonics Symposium Proceedings, 1975, pp 317-321.
11. W. S. Ishak and W. R. Shreve, "Low-Loss, Low-Ripple SAW Filters Using Group-Type Unidirectional Transducers," IEEE Ultrasonics Symposium Proceedings, 1981.

H. Edward Karrer

Ed Karrer is a graduate of Stanford University, receiving the BS and MS degrees in electrical engineering in 1959 and 1960. He came to HP in 1966 with experience in directing a measurement techniques group at another company's technology center. He was manager of the physical acoustics department in HP Laboratories for several years and now heads the applied technology and medical department. Ed is named as an inventor on five patents and is an author of 15 publications concerned with acoustic imaging, SAW devices, bulk resonators, and pressure and force sensors. He is a member of the IEEE and the American Institute of Ultrasound in Medicine. Ed was born in Brentwood, California and now lives in Palo Alto, California. He is married, has two teenage children and a Labrador retriever, and enjoys fishing and playing classical guitar (which he also teaches).

William R. Shreve

Bill Shreve was born in Dobbs Ferry, New York and attended Cornell University, earning a BS degree in engineering physics in 1969. He continued his studies at Stanford University, receiving the MS (1971) and PhD (1974) degrees in applied physics. Bill joined HP in 1978 with four years of industrial experience working with SAW technology. At HP he has worked on SAW resonators and is the project manager for the SAW program at HP Laboratories. Bill is named as an inventor on three SAW device patents and is an author of more than twenty papers related to SAW devices. He was an instructor for the Continuing Engineering Education Program at George Washington University. Bill is the founder and vice-chairman of the Santa Clara Valley Sonics & Ultrasonics Chapter of the IEEE, and a member of the IEEE Sonics & Ultrasonics Group Administrative Committee. He lives in Sunnyvale, California with his wife, two daughters, and the family dog. He enjoys jogging, hiking, woodworking, and gardening.

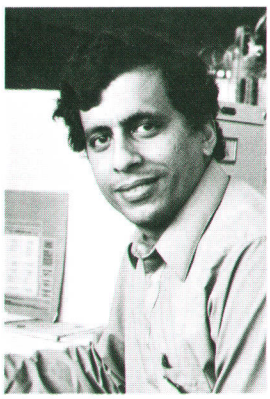

Waguih S. Ishak

Waguih Ishak joined HP in 1978 after completing post-doctorate work at McMaster University, Hamilton, Canada. A native of Cairo, Egypt, he earned a BS degree in electrical engineering at Cairo University in 1971 and a BS degree in mathematics at Ain Shams University in 1973. He taught physics at two universities in Cairo for two years and then attended McMaster University, earning the MS and PhD degrees in electrical engineering in 1975 and 1978. At HP he has worked on bubble memories and magnetic printers, and now is involved with SAW device technology. Waguih is a member of the IEEE and the Association of Professional Engineers of the Province of Ontario. He is an author of twelve publications dealing with bubble memory devices, numerical optimization, and SAW devices. He is married, has a son, and lives in Sunnyvale, California. His outside activities include being treasurer of the Coptic Orthodox Church in Hayward, California and playing soccer.

Surface-Acoustic-Wave Resonators

by Peter S. Cross and Scott S. Elliott

A SURFACE-ACOUSTIC-WAVE (SAW) delay line (see article on page 3) can be converted into a high-Q resonator filter by enclosing the interdigital transducers (IDTs) with two periodic arrays of grooves as shown in Fig. 1. Each array acts as an efficient reflector of surface waves over a band of frequencies determined by the groove period and depth. When two such arrays are placed near each other, a Fabry-Perot (laser-type) resonator is formed.[1]

Grating Reflectors

Because of its complex particle motion, a surface wave largely decomposes into reflected longitudinal and shear waves when incident upon an abrupt surface discontinuity such as a crystal edge. Therefore, to reflect surface waves back as surface waves efficiently, it is necessary to use an array of a large number of small periodic surface perturbations (typically shallow etched grooves) as shown in Fig. 2. Each edge of a groove has a small reflection coefficient r which is proportional to the groove depth. The efficiency of conversion into bulk modes is proportional to r^2 and is thus negligible for $r<<1$. At the frequency where the grating period is half the surface acoustic wavelength, the reflections from all N grooves in the array add coherently to give a power reflection coefficient $R=\tanh^2(2Nr)$. Thus R approaches unity as Nr is made large. The transmission coefficient T is just the complement of R (equal to $1-R$).

To calculate the reflection coefficient as a function of frequency, the grating can be modeled as a periodically mismatched transmission line as shown in Fig. 3.[2] The ridge and groove regions are characterized by acoustic admittances Y_0 and Y_1, respectively. Thus, there is a reflection at each edge caused by the admittance discontinuity. Also included in the model is a reactive element jB that is associated with evanescent bulk modes that are localized at each groove edge. The main consequence of this reactive energy is to shift the frequency f_r at which the peak reflection occurs. Since the magnitude of B is proportional to r^2 (and hence to the groove depth h squared), f_r and the resulting resonator center frequency f_0 shift as a function of h. Thus, although this effect makes it essential to maintain good groove depth uniformity across a substrate, groove depth adjustment can also be used to trim the frequency of a completed resonator.

The magnitude and phase of the reflection coefficient of a grating are shown in Fig. 4. The frequency dependence of the magnitude is very similar to a sin x/x function, but with a broadened and flattened central lobe whose width is proportional to r. The reflection phase has a nearly constant slope inside the main lobe and a sawtooth behavior in the sidelobe regions. The constant slope near the center frequency is mathematically equivalent to assuming that the distributed reflection from the grooves originates from a plane mirror located a fixed distance $\lambda_r/8r$ inside the grating (λ_r = wavelength at f_r).[3] As a result, the behavior of

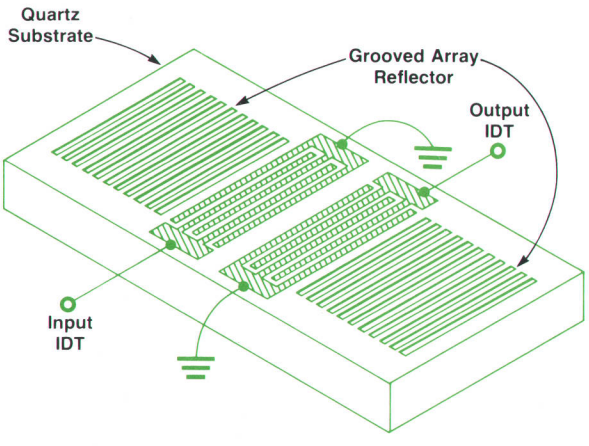

Fig. 1. *Two-port surface-acoustic-wave resonator. The arrays of grooves at each end reflect the surface waves excited by the input IDT. The reflected waves constructively add at a frequency largely determined by the periodicity of the grooves.*

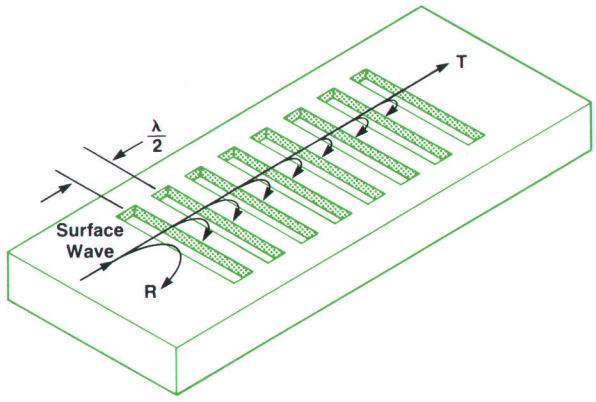

Fig. 2. *Simple surface-wave reflector using a periodic array of grooves etched to a depth h in the surface. R is the reflection coefficient and T is the transmission coefficient for an incident surface wave.*

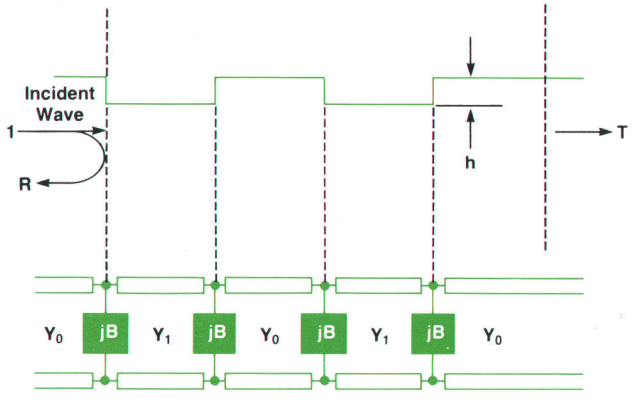

Fig. 3. *Equivalent circuit model for a grating reflector.*

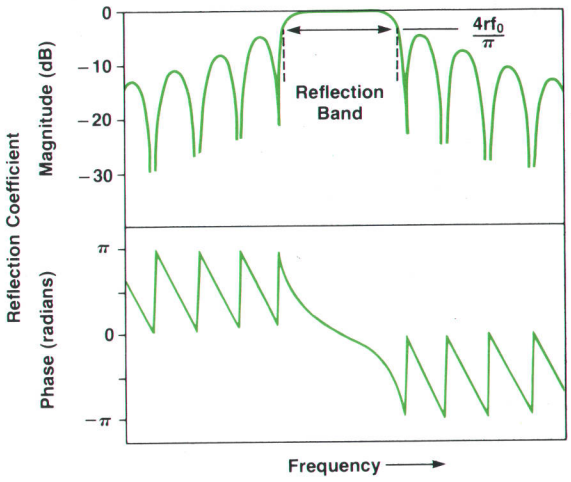

Fig. 4. *Magnitude and phase of grating reflection coefficient versus frequency. The width of the reflection band is proportional to groove depth h.*

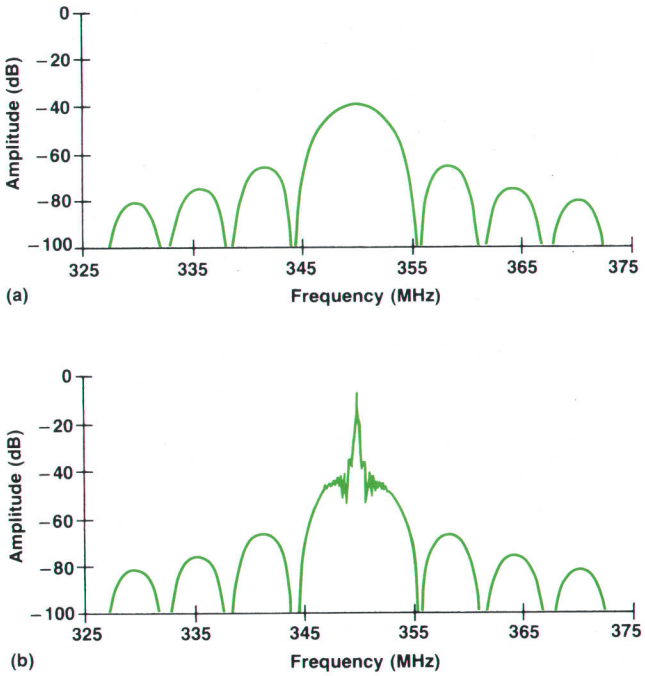

Fig. 5. *(a) Frequency response of a 350-MHz SAW delay line. By adding grating reflectors at each end, a resonant peak is obtained at the center frequency (b).*

the reflection grating can be considered to be the same as that of a localized plane mirror when making first-order calculations of resonator properties.

The effect of the gratings on delay-line response is shown in Fig. 5. Without the gratings, the delay line has a $(\sin x/x)^2$ response (for unapodized IDTs) with a relatively high insertion loss because the IDTs are weakly coupled to the substrate intentionally in a resonator configuration (Fig. 5a). With the addition of the gratings, the reflected surface waves make several passes through the cavity thereby increasing the effective coupling to the IDTs at resonance. The result is a narrow, low-insertion-loss peak that rises out of the delay-line response (Fig. 5b).

In the vicinity of the resonant peak, SAW resonators (SAWRs) are accurately modeled by a series RLC circuit as shown in Fig. 6.[4] The devices can have either one or two transducers and therefore have either one or two electrical ports as indicated. The one-port configuration has an equivalent circuit consisting of a series RLC branch shunted by C_0, the static capacitance of the IDT. This is identical to the equivalent circuit of a bulk crystal resonator. In practice, the reactance of the static capacitance often must be compensated by using an external inductor to ensure that oscillation at spurious frequencies does not occur. In the two-port configuration, the static capacitance individually shunts the input and output ports but not the resonant RLC arm. Thus, there is usually no necessity to compensate C_0 when using a two-port SAWR.

The ultimate performance of a SAW resonator is limited by the various cavity loss mechanisms which include viscous damping in the substrate, mode conversion in the gratings and resistive loss in the electrodes. Most of the loss

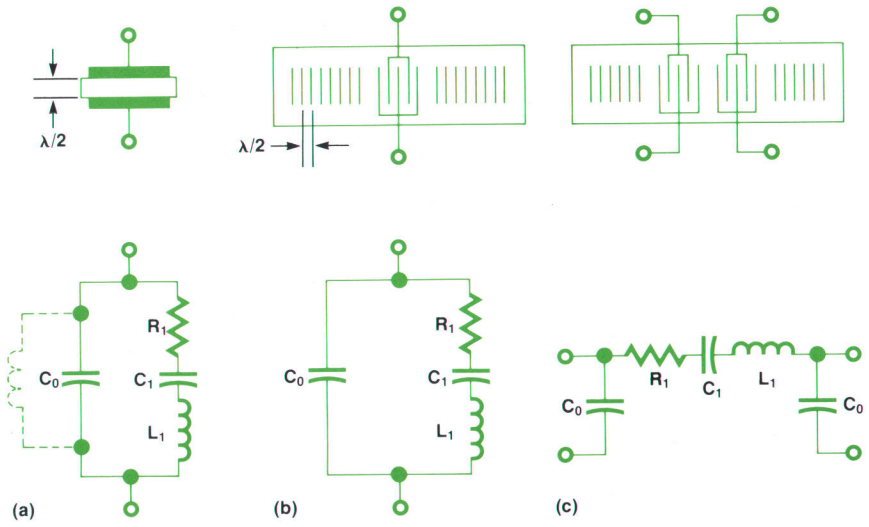

Fig. 6. *Crystal resonator geometries and equivalent circuits. (a) One-port, bulk-acoustic-wave resonator. (b) One-port surface-acoustic-wave resonator. (c) Two-port surface-acoustic-wave resonator.*

mechanisms vary directly with the geometrical features of the device and can be minimized by proper design. Viscous damping, however, cannot be eliminated and is therefore the fundamental limitation to resonator Q and insertion loss. The attenuation due to viscous damping increases as the square of the resonant frequency and causes the maximum achievable Q to fall at higher frequencies as shown in Fig. 7. Furthermore, if there is a restriction placed on the total allowable device length L, the Q also falls off at low frequencies because of increased transmission through the shorter gratings. Thus, the Q of SAWRs typically falls in the range of 5000 to 100,000.

The minimum resonant resistance for a single-mode resonator is plotted as a function of frequency in Fig. 8 on page 14. The curves are essentially inverted replicas of the Q-curves in Fig. 7 except that the minimum resistance rises very rapidly (as $f^{2.5}$) at higher frequencies. The rapid rise occurs because, in addition to increased viscous damping, there are constraints on the minimum IDT metal thickness and groove depth (taken as 30 nm in Fig. 8) obtainable in a practical situation. These constraints limit the transducer size (and coupling strength) allowable for single-mode operation which in turn causes high values of resonant resistance for frequencies above 1 GHz.

(continued on page 13)

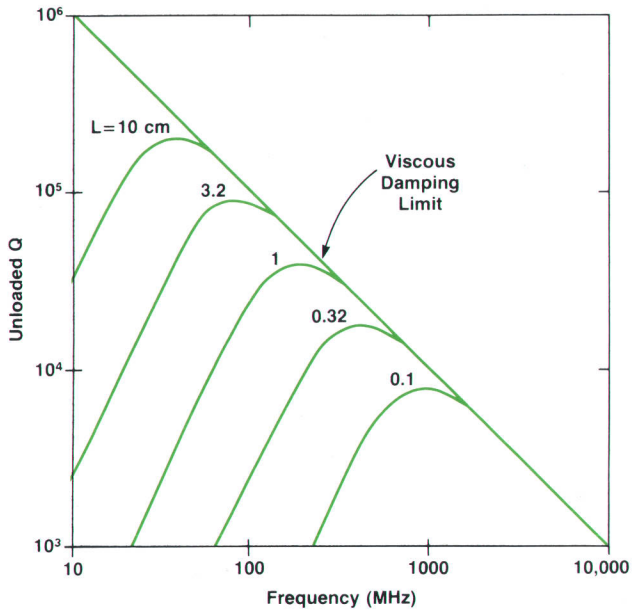

Fig. 7. *Unloaded Q versus frequency as a function of the length L of a quartz surface-acoustic-wave resonator.*

SAWR Fabrication

by Robert C. Bray and Yen C. Chu

To be competitive economically, surface-acoustic-wave resonators (SAWRs) must be fabricated using standard photolithographic and thin-film techniques. A complete device consists of aluminum thin-film interdigital transducers (IDTs) that are precisely positioned with respect to an array of etched grooves on the polished surface of a piezoelectric quartz crystal. In the UHF range (300 to 3000 MHz) where SAWRs find most applications, the patterns have linewidths of a few micrometres or less (e.g., 1-μm-wide lines and spaces correspond to a resonant frequency of about 800 MHz). Thus, the fabrication process described below (see Fig. 1) was devised to allow definition of the IDTs and gratings by a single, high-resolution photolithographic step to avoid difficult, if not impossible, pattern alignments.

The process starts with a highly polished 5-cm-diameter, 0.5-mm-thick wafer substrate of single-crystal quartz on which a number of devices can be fabricated simultaneously. The wafer is cut from the crystal boule at a precise angle that is chosen to give a zero delay temperature coefficient at a given temperature. The backside of the wafer is roughened to reduce specular reflection of any bulk acoustic waves that may be excited by the surface wave transducer.

Because the polished surface and the crystalline structure of the substrate are important, the wafers are inspected before processing begins by etching the quartz surface slightly so that any crystal defects are delineated.

The photolithography is done using standard photoresist processing with the mask-to-wafer pattern transfer done by using an aligner that brings the wafer and mask into intimate contact. Linewidth variations must be kept within 5% across the wafer to reduce the spread in resonant frequencies to an acceptable tolerance. Because the quartz is so highly polished and the patterned lines are so narrow, adhesion of the photoresist is often a problem. To promote adhesion and to reduce reflections during exposure, a 5-nm-thick titanium layer is first deposited by electron beam deposition.

After painstaking cleaning, a 0.4-μm thick layer of photoresist is spun on the wafer. The negative image of the interdigital transducer and grating patterns is defined by contact exposure. To facilitate good lifting after the aluminum evaporation later, the photoresist is given an overhang structure (Fig. 2) with a chlorobenzine soak before development. After development the exposed portion of the underlying titanium is etched away, leaving fresh areas of the quartz surface for the aluminum deposition.

After the photoresist is baked, copper-doped aluminum is deposited at a very slow rate to a precisely controlled final thickness. Aluminum is chosen as the metallization in the IDT region because its acoustic impedance closely matches that of quartz. Reflections from fingers of any other metal would be unacceptably large for a high-Q SAWR. Copper doping is used to strengthen the aluminum and prevent metal migration that is observed at the high power dissipation desirable for low-phase-noise oscillators.

The remaining photoresist is softened and lifted off the surface of the wafer by soaking the wafer in acetone. This removes the unwanted aluminum layer overlying the resist, leaving behind the desired pattern on the quartz surface. Then the wafer is covered with a new layer of photoresist which is patterned and developed to protect the IDT regions from further etching. Using the exposed parts of the aluminum pattern for a mask, the grating reflector

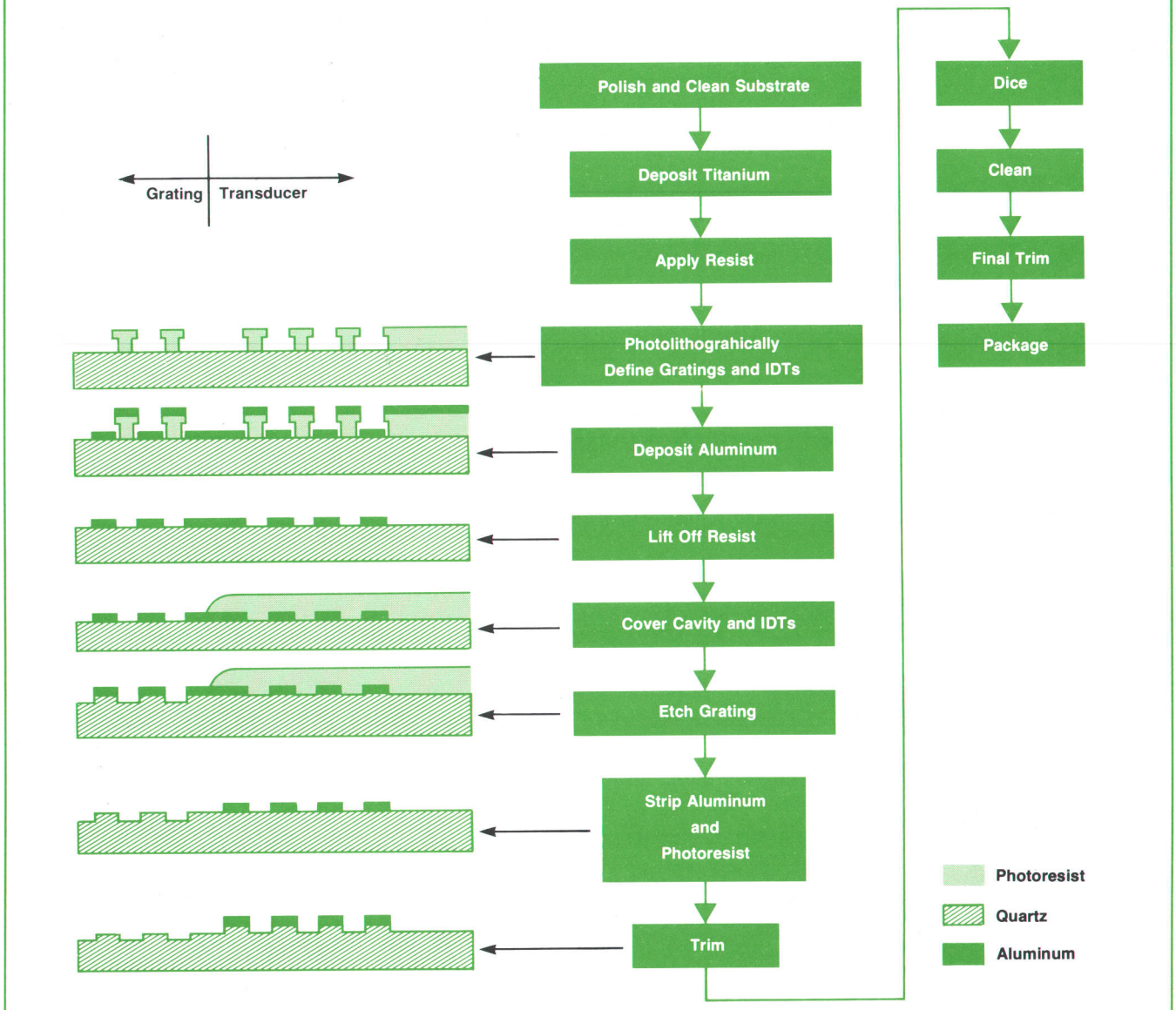

Fig. 1. *Fabrication process for SAW resonators.*

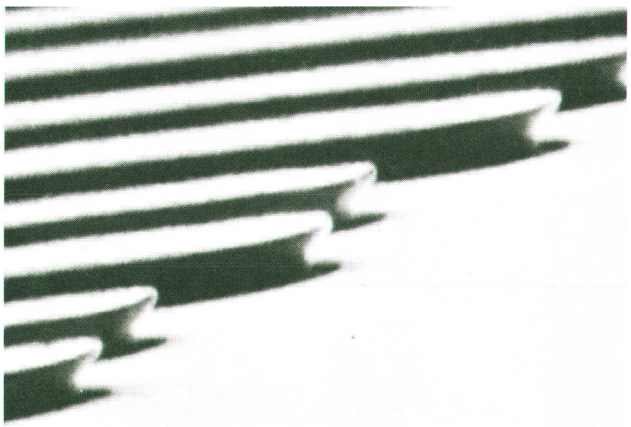

Fig. 2. *Scanning electron microscope photograph of photoresist pattern showing overhang structure desired for good aluminum liftoff patterning.*

grooves are etched into the quartz with a $CF_4/0_2$ reactive ion etching (RIE) process. Good control of all process parameters (pressure, gas flow rates and RF power) is the key to uniform, repeatable groove etching. After the grooves are etched the exposed aluminum is removed and then the resist protecting the IDTs is stripped.

Gold bonding pads are required for making contact to the external world. To avoid the formation of gold-aluminum intermetallic compounds, titanium-platinum transition layers are deposited between the IDTs and the surface of the bonding pads.

At this point in the process the devices are functional and can be tested to determine the average resonant frequency on the wafer. The resonant frequency is highly sensitive to IDT metal thickness and grating groove depth. For example, an 800-MHz SAWR designed with aluminum fingers 45-nm thick varies by 500 kHz or 620 ppm in center frequency as the IDT metal thickness varies between 40 and 50 nm. For this reason, it is usually necessary to trim the devices to achieve acceptable yields for an inital frequency specification of ±50 kHz or better. This trimming is accomplished by placing the entire wafer back into the RIE sys-

Yen C. Chu

Yen Chu was born in Kiangsu, China and attended Chen-Kung University, Taiwan, earning a BS degree in Physics in 1967. He received the MS degree in solid-state physics from the University of Iowa in 1970 and the MS degree in metallurgy and material science from the University of Florida in 1972. Yen joined HP in 1975 with previous experience working with gallium arsenide materials. At HP he has worked with GaAs FETs and YIG crystals, and contributed to the development of the SAWR fabrication process. Yen is now working on IC process improvements. He is the author of one paper on SAWR device aging and a co-author of three other papers concerned with SAW devices. Yen is married and has two children, a girl and a boy. He lives in Cupertino, California and enjoys spending his leisure time gardening.

Robert C. Bray

Bob Bray is a native of Detroit, Michigan and received the BS (1966) and MS (1967) degrees in physics at the University of Michigan. He taught physics in a Michigan high school until 1977 when he began graduate studies in electrical engineering at Stanford University, earning the MSEE and PhDEE degrees in 1979 and 1981. Bob joined HP this year and is involved with SAW device design, processing, and aging studies. He has authored four papers on acoustic microscopy and SAW device physics and is a member of the IEEE and the Acoustical Society of America. Bob is married, has two sons and a half-wild cat, and lives in Santa Rosa, California. He enjoys camping, hiking, listening to classical music, and attending as many old movies, concerts, plays, and operas as he can when he is not busy reading stories to his boys.

tem and using the IDT metallization as a mask. As a result, the IDTs are effectively raised up on quartz pedestals which increases the stored energy in the IDT region and lowers the resonant frequency.[1]

Next the wafer is sawed into individual devices which are cleaned and heat treated. The individual SAWRs can now be given a final frequency trim before packaging.

The finished chips are ribbon bonded to a thick-film ground plane on a ceramic substrate, and wire bonded to the connector pins. A nickel lid is brazed on after heat treatment in vacuum.

Acknowledgments

Developing a microelectronic fabrication process requires the insights gained from the combination of many diverse talents. Among the individuals contributing to this process are Pete Planting, Don Johnson, T. S. Tan, Sandy Giannotti, George Henry, John Ratcliff, Catherine Johnsen and Michael Symons.

Reference

1. P.S. Cross and W.R. Shreve, "Frequency Trimming of Surface Acoustic Wave Devices," U.S. Patent #4,278,492.

SAWRs versus Bulk-Acoustic-Wave Resonators

Although fundamental-mode SAW oscillators are sometimes compared to multiplied bulk-acoustic-wave (BAW) oscillators at the same frequency, SAW and BAW resonators address different frequency ranges and thus are not directly competing technologies. BAW crystals are useful in the range of 100 kHz to 50 MHz for the fundamental resonance mode. They are limited in frequency on the low end by large size and high loss. Because fundamental-mode crystals must be cut to a thickness of one-half wavelength, they are limited at the high-frequency end by the fragility of the thin crystal. Mechanical overtones of odd order may be used to extend the useful frequency range to around 300 MHz, but problems with unwanted nearby modes become severe.

SAW resonators begin to be useful right where BAW devices are limited (at 50 MHz) and span the frequency range up to about 1 GHz. Large size is again the limiting factor on the low end; at 50 MHz, one SAW resonator occupies an entire 5-cm-diameter quartz wafer. At 1 GHz, the dimensions for the IDT fingers and grooves become prohibitively small for photolithographic processing techniques. Devices have been demonstrated up to 2.6 GHz using submicrometre electron-beam lithography.[5] The loss caused by material viscosity increases rapidly with frequency and dominates at frequencies above 1 GHz.

Typical parameters of interest for one-port SAWRs and BAWRs are compared in Table I. Above 1 MHz, the unloaded Q in either case falls off with frequency. The circuit parameters R_1 and C_0 are comparable for both types of resonators. Bulk-wave crystals exhibit better performance in the areas of temperature stability and long-term stability. The AT-cut of quartz supports bulk waves that have a near-zero temperature coefficient at room temperature with variations of about ± 5 ppm in the 0° to 55°C range. The recently developed SC-cut offers still better performance.[6] The best temperature stability to date for SAW devices occurs for the ST-cut of quartz. The temperature drift is a parabolic function with a zero linear temperature coefficient near 25°C (depending on the exact cut angles with respect to the crystal axes). The quadratic temperature coefficient is approximately $+35\times10^{-9}$ per °C squared away from the turnover temperature, corresponding to a drift of ±15 ppm over a range of 0° to 55°C.

Temperature-controlled, bulk-wave crystal oscillators are usually chosen for precision frequency applications because of the extremely good long-term stability (aging rate) of BAW resonators. Aging drifts of less than 0.1 ppm per year are obtainable. SAW resonators typically age at rates between 1 and 10 ppm/year.

One of the major advantages of SAW devices is the easy access to the acoustical energy along the signal path. It is possible to choose the shape of the frequency response and placement of the spurious modes by correct positioning of the transducer electrodes and grating grooves. Access to the surface waves also allows for a two-port, resonator-filter design (Fig. 1). Because the capacitance between the two IDTs is low, high rejection occurs away from the resonant

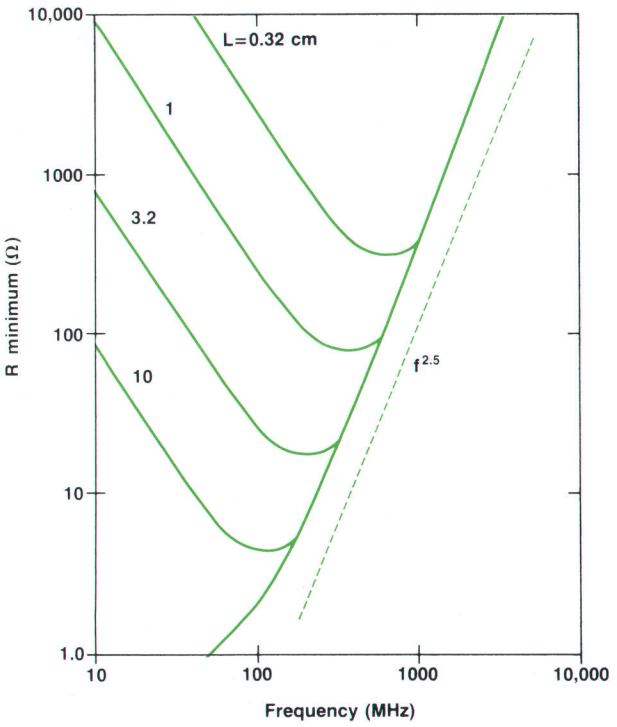

Fig. 8. *Minimum resonant series resistance versus frequency for a single-mode quartz SAWR as a function of device length L.*

frequency, eliminating the need for external filters in oscillator design.

The low cost and high availability of bulk-wave crystals are a result of the maturity of that technology. SAW resonators have been introduced only recently in the manufacturing environment (see box on page 15). BAWRs and SAWRs are about the same size, but the latter can be fabricated by planar, photolithographic processing techniques (see box on page 11), as opposed to the careful machining and polishing processes required for BAWRs. With continued process development and growing demand, it is our belief that SAW resonators will soon be as inexpensive and numerous as their BAW counterparts.

SAW Oscillators

SAW resonators are used primarily as frequency-control devices in oscillators. The advantages of using a SAWR rather than alternative frequency-controlling schemes (e.g. LC circuits, coaxial delay lines and metal cavity resonators) are high Q, low series resistance, small size and good frequency stability. These attributes allow the design of small, highly stable oscillators of high spectral purity in the 50 MHz to 1 GHz range.

The design of oscillators using bulk-wave resonators was discussed in a previous HP Journal article.[7] It was noted therein that frequency multiplication causes phase noise and sidebands to increase by 20 dB for every decade of multiplication. To achieve low phase noise in the 50 MHz to 1 GHz range, it may thus be advantageous to use a fundamental-mode, SAW-controlled oscillator rather than the usual multiplied output of a crystal-controlled oscillator. As an added benefit, fewer parts are needed because of the elimination of the multiplying circuitry.

The most commonly used SAWR oscillators are of the common-emitter (or Pierce) type and the common-base type as illustrated in Fig. 9. This figure depicts oscillators using

(continued on page 16)

Table I

Comparison of surface-acoustic-wave resonators (SAWRs) and bulk-acoustic-wave resonators (BAWRs).

Parameter	BAWR Frequency			One-Port SAWR Frequency		
	Low[a,b]	Medium[b]	High[a,b]	Low	Medium	High
f_o (MHz)	1	10	50	50	500	1000
Q	2 to 20×10^5	1 to 10×10^5	8 to 20×10^4	8 to 15×10^4	12 to 20×10^3	8 to 10×10^3
$R_1(\Omega)$[c]	10 to 300	25 to 100	25 to 100	25 to 50	20 to 50	100 to 250
C_o (pF)		4 to 8		10 to 20	2 to 4	1 to 2
Aging (ppm/year)		0.01 to 5			1 to 10	
Maximum Power Dissipation (dBm)	−10	−15	−20		3[f]	
$\Delta f/\Delta T$ for 0° to 55°C (ppm)		±5[d]			±15[e]	
Size (cm)	1	1	<1	5	1	<1

Notes:
a. Data provided by E. Morgan and T. Schuyler, Colorado Crystal Inc., and J. Holmbeck, Northern Engineering, Inc.
b. Data provided by J.A. Kusters, Hewlett-Packard Co.
c. R_1 is very temperature dependent for BAWRs. Data is for 25°C.
d. AT-cut quartz
e. ST-cut quartz
f. Maximum power dissipation is closely related to long-term stability so this value may have to be reduced to approach the very low aging rates of BAWRs.

280-MHz Production SAWR

by Marek E. Mierzwinski and Mark E. Terrien

HP's Santa Rosa Technology Center has recently introduced the first production surface-acoustic-wave resonator (SAWR) developed for use in a Hewlett-Packard instrument.[1] The SAWR is a single-port, dual-transducer device (see Fig. 1) resonant at 280 MHz (f_0) with a typical packaged Q of 18,000 and a typical spurious response of −8.5 dB at $f_0 \pm 300$ kHz.

Although the individual processing steps required to manufacture, test, and package a surface-acoustic-wave resonator are similar to those required to produce semiconductor devices, the unique properties associated with a surface-wave device did create many manufacturing problems. The processing steps, the test procedures, and the packaging scheme were all developed so that the resonator would be an easily fabricated, price-competitive drop-in replacement for an overtone bulk-wave crystal resonator.

The original application for this device was as a direct replacement for a bulk-wave crystal resonator used at its 11th overtone. The device was put into a hermetically sealed, nickel-plated package that had a standard crystal configuration (Fig. 2). This device is supported by a gold ribbon bonded to two 1-mm-diameter pins and is sealed in nitrogen with a resistance weld to a hermeticity leak rate less than 10^{-8} standard cc of helium per second.

Cleanliness is extremely important in the assembly and sealing process because any conductive particles larger than 2 μm in diameter can potentially short adjacent transducer electrode fingers. The device cannot be passivated since the SAW energy is confined to the surface of the quartz. A passivation layer would increase the insertion loss and lower the Q by damping the wave. Even a monolayer of certain types of residue alters the electrical performance by an unacceptable amount. Thus, all the processing and testing must be done in a very clean environment. The delicate, thin, aluminum transducer electrode pattern will not allow vigorous cleaning to remove contamination once it is introduced.

The SAWRs are operated as one-port devices by bonding the two interdigital transducers (IDTs) in parallel. They can be modeled with the equivalent circuit shown in Fig. 6 on page 10. All devices must meet the following specifications:

Parameter	Minimum	Typical	Maximum
Resonant Frequency f_0 (MHz)	279.860	280.000	280.140
Resonant Series Resistance R_1 (Ω)		35	60
IDT Interfinger Capacitance C_0(pF)	2.0	2.5	3.0
Unloaded Q	10,000	18,000	
Spurious Mode Response (dB) ($f_0 \pm 300$ kHz)	−6	−8.5	

Two-port prototype packaged devices have a series resonance resistance of less than 240 ohms and one-half of the one-port interfinger capacitance per port. All measurements are made in a 50-ohm system using an HP 1000 Computer that controls an HP Model 8410 Network Analyzer and an HP Model 8660A Frequency Synthesizer via an HP-IB interface. Because of the difficulties in wafer processing and the stringent center frequency requirements, 53% of the devices are rejected before the packaging state. 85% of the remaining devices are successfully packaged and go into stock. The absolute maximum continuous RF power dissipation is +3 dBm. The packaged devices easily withstand the 30g shock and 75°C maximum internal operating temperature tests to which HP instruments are subjected.

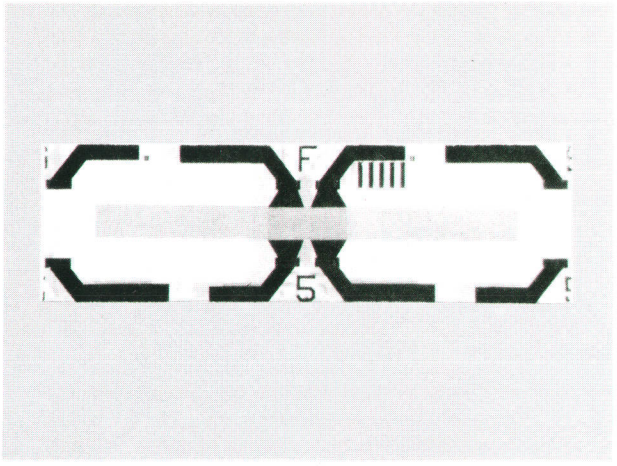

Fig. 1. *Microphotograph of HP 280-MHz one-port surface-acoustic-wave resonator.*

This SAWR was originally designed as a pin-for-pin replacement for a harmonic bulk-wave crystal in a Colpitts-type oscillator used in the HP Model 8558B and 8568A Spectrum Analyzers. The device provides a frequency-controlled feedback path from a capacitive ladder network to the input of a bipolar transistor. The main benefits of the SAWR in this application are improved spurious response and a lower series resonance resistance. Fig. 3

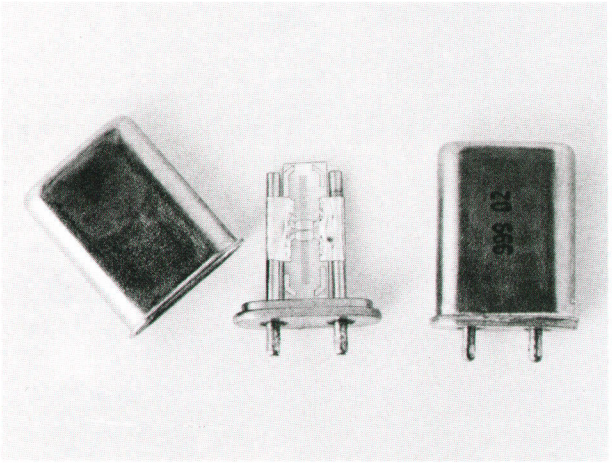

Fig. 2. *The SAWR shown in Fig. 1 is packaged in a standard crystal package as shown above.*

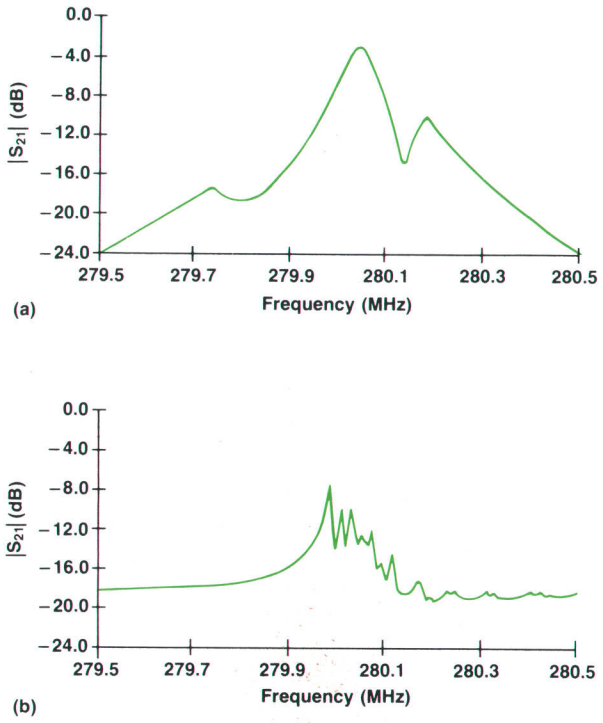

Fig. 3. *Frequency response for (a) a typical 280-MHz one-port SAWR compared to (b) a typical eleventh-overtone bulk-acoustic-wave crystal.*

displays the frequency response of a typical 280-MHz SAWR and the bulk-wave crystal it replaces. The improved close-in spurious response of the SAWR decreases the oscillator's phase noise. The spur at f_0+300 kHz is a transverse cavity mode that could be suppressed by a simple redesign of the IDTs. However, the spur causes no degradation of the oscillator performance for the current application and so a redesign is unnecessary. Precise fabrication control allows predetermination of the amount of feedback needed for oscillation and the amount of inductance needed to resonate out the interfinger capacitance.

As a direct replacement the SAWR must be packaged as a one-port device. This results in decreased out-of-band rejection and higher bypass interfinger capacitance. New applications could use a two-port configuration, which offers much better off-resonance rejection and eliminates the need to tune out the bypass capacitance. The 280-MHz SAW device can be used to provide frequency stability for any oscillator configuration or filtering in many circuit designs.

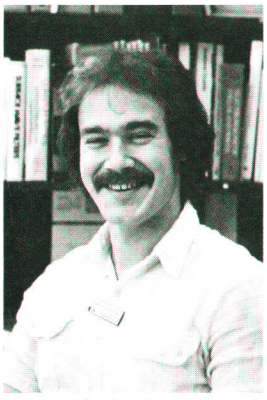

Mark E. Terrien

Mark Terrien joined HP in 1980 as an applications engineer working with SAW devices, GaAs components, varactors, and YIG products. He is a native of Milwaukee, Wisconsin where he attended the University of Wisconsin to earn a BS degree in applied mathematics and physics in 1978. Mark then studied for an MSEE degree at the Madison campus of the University of Wisconsin and received it in 1979. He is a member of the IEEE and Phi Beta Kappa. Mark lives in Santa Rosa, California with his four guitars and enjoys playing jazz-rock, driving automobiles, tasting the local Sonoma County wines, and outdoor activities.

Marek E. Mierzwinski

Marek Mierzwinski is a production engineer for microwave power transistors and SAW devices and joined HP in 1979 after he received a BS degree in applied and engineering physics from Cornell University. He is currently working toward an MSEE degree at Stanford University through a cooperative work-study program. Marek has co-authored several articles on SAWRs. He is a native of Connecticut (born in Waterbury), single, and lives in Santa Rosa, California. He is a member of the Polish-American Club, serves as president of the HP Bicycle Club, and enjoys photography.

Acknowledgments

Many people contributed to the development of the 280-MHz SAWR, among them are Melody Bellagio, Dave Bennie, Dixie Feenan, Norm Gri, Kevin Kerwin, Lynn Moughmer and Deanna Schramm.

Reference

1. S. Elliott, M. Mierzwinski and P. Planting, "Production of Surface Acoustic Wave Resonators," IEEE Ultrasonics Symposium Proceedings, 1981.

two-port SAWRs, rather than one-port, to make the need for further filtering unnecessary. In the common-emitter oscillator of Fig. 9a the SAWR provides resonant feedback from the collector to the base. Inductors are used to remove the reactance (at resonance) caused by IDT capacitance. The impedance and admittance elements Z_1, Y_1, Z_2 and Y_2 are chosen to transform the impedances between the SAWR and the transistor for optimum power transfer and the lowest phase noise. Low phase noise is achieved by maximizing the power transfer through the SAW device while retaining a high loaded Q.

The common-base configuration (Fig. 9b) has potentially less noise near the frequency of oscillation because no noise signal can be present at the base, which avoids the high noise current gain between base and collector. However, this oscillator is only conditionally stable which leads to the possibilities of spurious oscillations, squegging, and a higher noise floor far away from the fundamental signal than exhibited by the common-emitter oscillator. The SAWR provides feedback between the emitter and the collector. Since the current gain is less than unity, the LC network transforms the impedance of the SAWR at the collector to achieve a power gain large enough to cancel the losses in the loop. These elements are also selected to ensure high power transfer and a zero phase condition around the loop.

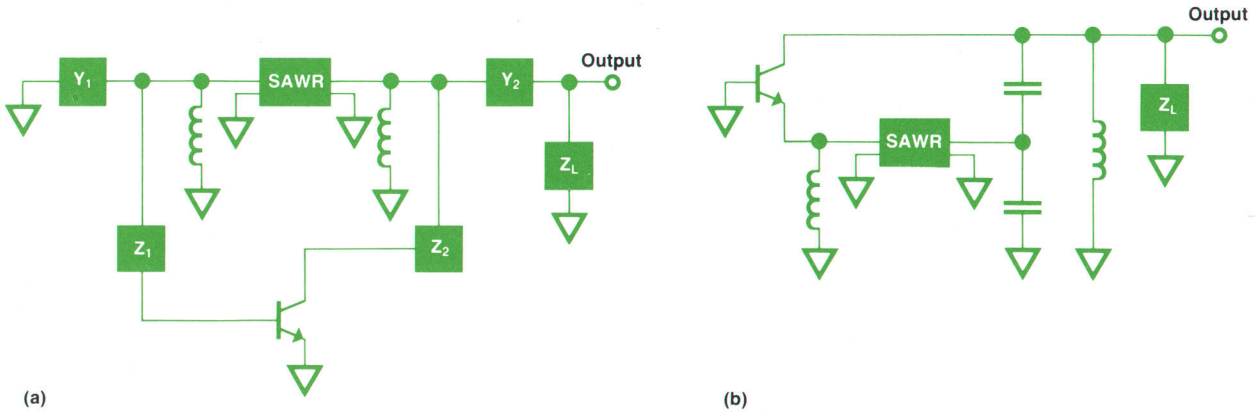

Fig. 9. *SAW oscillators using two-port SAWRs in a common-emitter or Pierce circuit (a) and a common-base circuit (b).*

These two oscillator configurations exemplify the manner in which the well-established technology of bulk-wave resonators can be readily translated into the UHF range (300 to 3000 MHz) by the use of SAW resonators.

Acknowledgments

The authors wish to acknowledge the substantial contributions to the establishment of SAWR technology at Hewlett-Packard made by Weldon H. Jackson. We are also indebted to Roger Muat for many helpful discussions about oscillator design.

References

1. E.J. Staples, J.S. Schoenwald, R.C. Rosenfeld and C.S. Hartmann, "UHF Surface Acoustic Wave Resonators," IEEE Ultrasonics Symposium Proceedings, 1974, pp. 245-252.
2. E.K. Sittig and G.A. Coquin, "Filters and Dispersive Delay Lines Using Repetitively Mismatched Ultrasonic Transmission Lines," IEEE Transactions on Sonics & Ultrasonics, Vol. SU-15, No. 2, April 1968, pp. 111-119.
3. P.S. Cross, "Properties of Reflective Arrays for Surface Acoustic Resonators," IEEE Transactions on Sonics & Ultrasonics, Vol. SU-23, No. 4, July 1976, pp. 255-262.
4. W.R. Shreve, "Surface Wave Two-Port Resonator Equivalent Circuit," IEEE Ultrasonics Symposium Proceedings, 1975, pp. 295-298.
5. P.S. Cross, P. Rissman, and W.R. Shreve, "Microwave SAW Resonators Fabricated with Direct-Writing Electron-Beam Lithography," IEEE Ultrasonics Symposium Proceedings, 1980, pp. 158-163.
6. C.A. Adams and J.A. Kusters, "The SC Cut, a Brief Summary," Hewlett-Packard Journal, Vol. 32, No. 3, March 1981, pp. 22-23.
7. J.R. Burgoon and R.L. Wilson, "SC-Cut Quartz Oscillator Offers Improved Performance," ibid., pp. 20-29.

Peter S. Cross

Peter Cross joined HP in 1978 as a member of the technical staff at HP Laboratories and now is a project manager for integrated optical modulators and pressure sensors. He is a native of Los Angeles, California and attended the California Institute of Technology, earning a BSEE degree in 1968. Peter continued his studies at the University of California at Berkeley to receive the MSEE degree in 1969 and the PhD degree in 1974. Before joining HP he did research in integrated optics and SAW devices. Peter has taught basic electronics and semiconductor device physics and was an acting assistant professor at U.C. Berkeley in 1974. He is named as an inventor on four patents and has authored or co-authored over 20 papers on optics and microwave acoustics. He is a member of the IEEE and the Optical Society of America. Peter and his wife live in Palo Alto, California and are expecting their first daughter in January 1982.

Scott S. Elliott

Scott Elliott received the BSEE and MSEE degrees from the University of California at Berkeley in 1969 and 1971. After several years of directing R&D work on microwave filters and oscillators he resumed his education at the University of California at Santa Barbara, earning the PhDEE degree in 1979. Scott came to HP in 1978 as a development engineer for SAW and GaAs devices. He now is a project manager for surface acoustic wave technology. Scott is a member of the IEEE and has authored or co-authored over 20 publications concerned with SAWs, quantum electronics, and microwave ferrite components. A native of Aberdeen, Washington, Scott lives in Sebastopol, California with his wife, new son, dog, cat, and a sheep. He enjoys winetasting, camping, listening to jazz, home computers, and woodworking (he recently remodeled his home).

Physical Sensors Using SAW Devices

by J. Fleming Dias

A TYPICAL SURFACE-ACOUSTIC-WAVE (SAW) delay line as described on page 3 has two interdigital transducers (IDTs) that are photolithographically defined on an ST-cut quartz substrate with a known separation between them. If this delay line is stretched along the propagation direction or bent as a cantilever beam, the surface of the substrate becomes stressed. The surface stress causes an elongation of the substrate which in turn increases the center-to-center distance between the two IDTs. Moreover, if the level of the stress is high, the elastic constants and density of the material change, causing the value of the surface-wave velocity v_s to change. Elongation and velocity changes are also brought about by changes in the ambient temperature. These parameter changes allow a SAW delay line to function as a temperature, pressure, force, or displacement sensor. A rather elegant method of using a delay line in a practical sensor is to introduce it in the feedback loop of an amplifier to obtain an oscillator whose frequency is a function of the surface stress.[1,2]

Fig. 1 shows the schematic representation of a delay line oscillator, in which the total phase shift around the loop is given by

$$\sum\phi=\phi_0\pm\Delta\phi_0\pm\phi_{ex} \qquad (1)$$

where $\phi_0=\omega\tau=2\pi fL/v_s$ is the phase shift experienced by a wave traveling from an input IDT to a similar IDT situated a distance L from it. $\Delta\phi_0$ is the incremental phase shift caused by stressing the substrate and/or changing its temperature. ϕ_{ex} is the extra phase shift introduced by the amplifier and matching network. The phase shift ϕ_0 through the delay line is usually much greater than ϕ_{ex}. When $\sum\phi=2n\pi$ (n is an integer) and the total insertion loss around the loop is less than the amplifier gain, the system oscillates. The oscillator generates a comb of frequencies given approximately by nv_s/L. Due to the inherent sin x/x response of a simple IDT, only some of the modes are sustained and in practice only one mode at a time will be excited because of nonlinearities in the amplifier.

For a given mode, any perturbation in the loop phase forces the system to alter the oscillator frequency to compensate for this change by adjusting the total phase shift to be a multiple of 2π. From equation (1) the oscillator frequency will change when L and v_s are altered (assuming that ϕ_{ex} remains constant). In crystalline quartz, the fractional change in SAW velocity is a small factor compared to the surface strain caused by an elongation in L. We can therefore expect a decrease in oscillator frequency when L is increased by applying direct axial tension to the substrate.

An oscillator of the type described above also undergoes an undesired change in frequency with temperature as shown in Fig. 2. The parabolic nature of the curve forces one to operate the sensor at the turnover temperature where there is a reduced effect on the frequency. In the early years of SAW development, Jack Kusters at HP computed the turnover temperatures of several rotated Y-cuts of quartz and those results are shown in Fig. 3. For comparison, the experimental results obtained later are also shown.

A force transducer was built using a cantilevered structure as shown in Fig. 4 where the surface acoustic wave propagates in the X-direction of a rotated Y-cut quartz substrate. The free end of the cantilever was loaded with known weights and the frequency of the oscillator was measured as a function of the total weight.

Even though the crystal cut was chosen to yield a turnover point near room temperature, the variation of the oscillator frequency with temperature was still a major limitation. Thus, to obtain an improved degree of temperature stability and double the force sensitivity, surface waves were propagated on both faces of the substrate using two pairs of IDTs. The IDTs located on opposite faces were offset

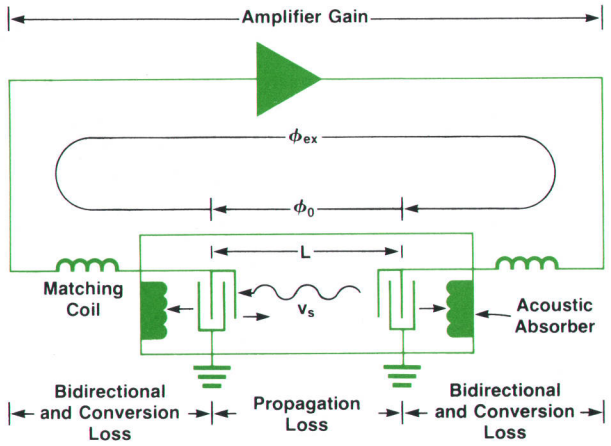

Fig. 1. *Simplified schematic of an oscillator using a SAW delay line as the feedback component.*

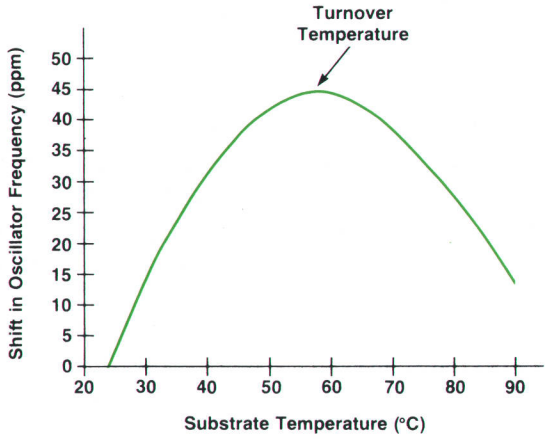

Fig. 2. *Frequency shift versus temperature for a crystal. The point where the shift reverses direction is called the turnover temperature.*

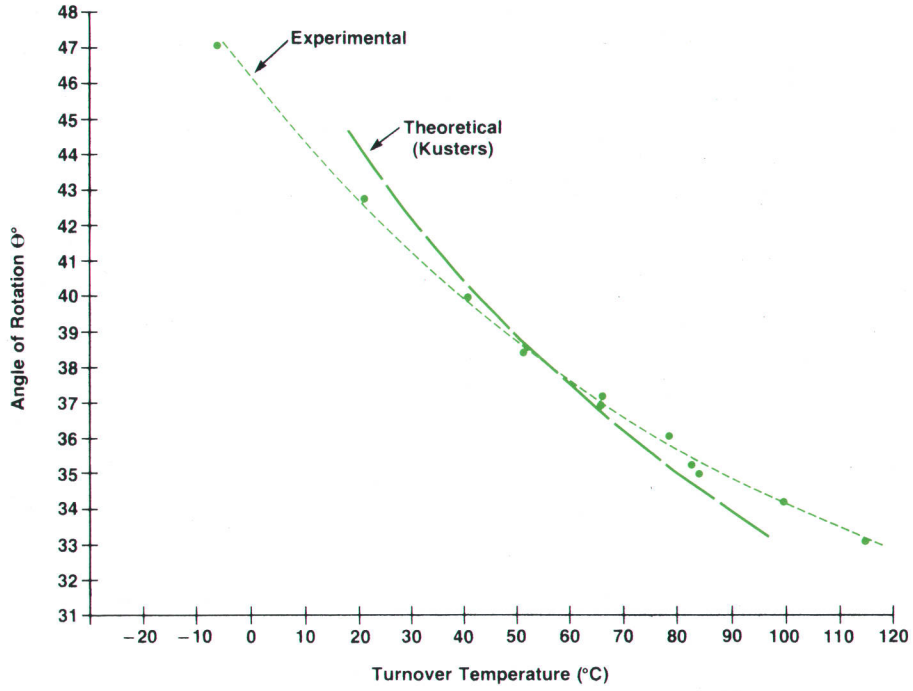

Fig. 3. *Turnover temperature versus crystal cut angle of rotation for Y-cut α-quartz.*

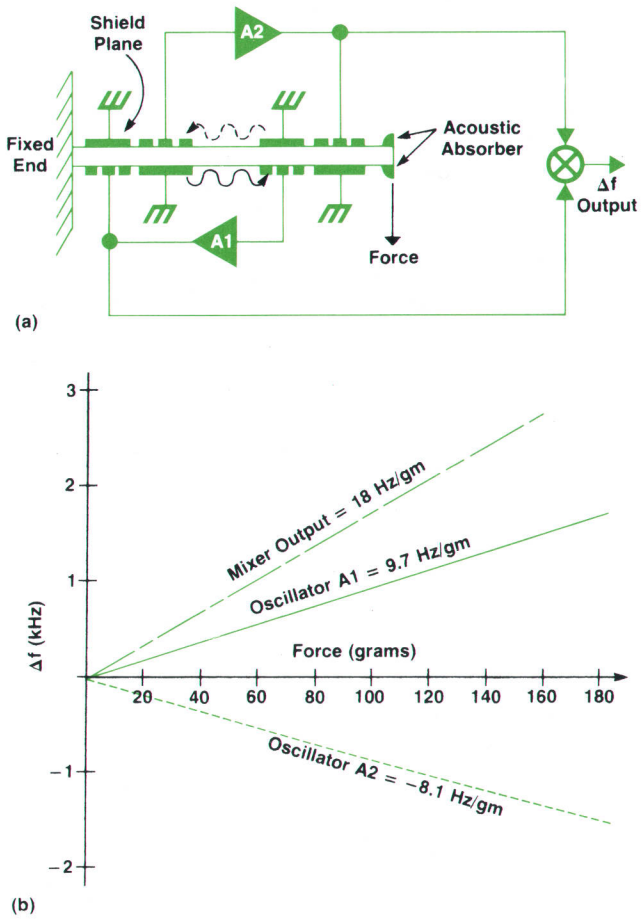

Fig. 4. *(a) Basic configuration of a force sensor using a cantilevered substrate with SAW delay lines on opposite faces. The responses for each SAW delay line oscillator and their difference are shown in (b).*

to minimize crosstalk, and ground-plane shields were included as shown. Each side was associated with a separate oscillator. When the substrate was deflected, one of the surfaces was under tension and the other in compression. Hence, the corresponding shifts in oscillator frequencies were in opposite directions. Changes in frequency caused by temperature variations, however, were in the same direction. When the oscillator outputs were mixed electronically and the difference frequency was monitored, we observed, as shown in Fig. 4b, the double force sensitivity that we expected and a very reduced sensitivity to temperature. Fig. 5 shows a complete force transducer using the double oscillator configuration.

Using similar schemes, pressure transducers were built

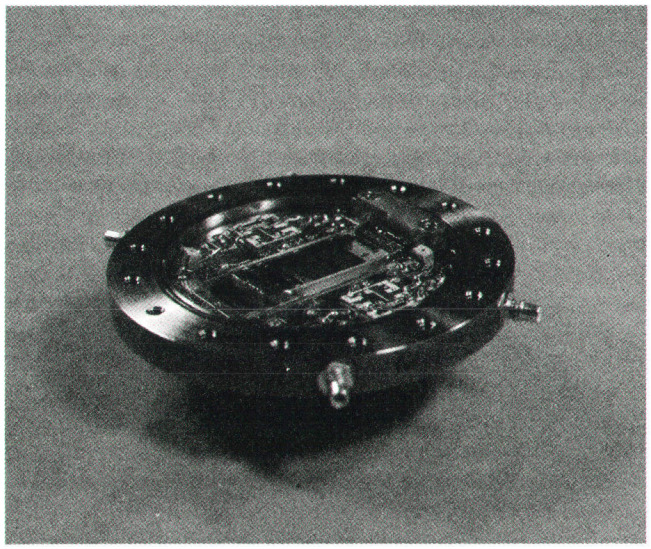

Fig. 5. *Photograph of a complete force sensor using double-oscillator design.*

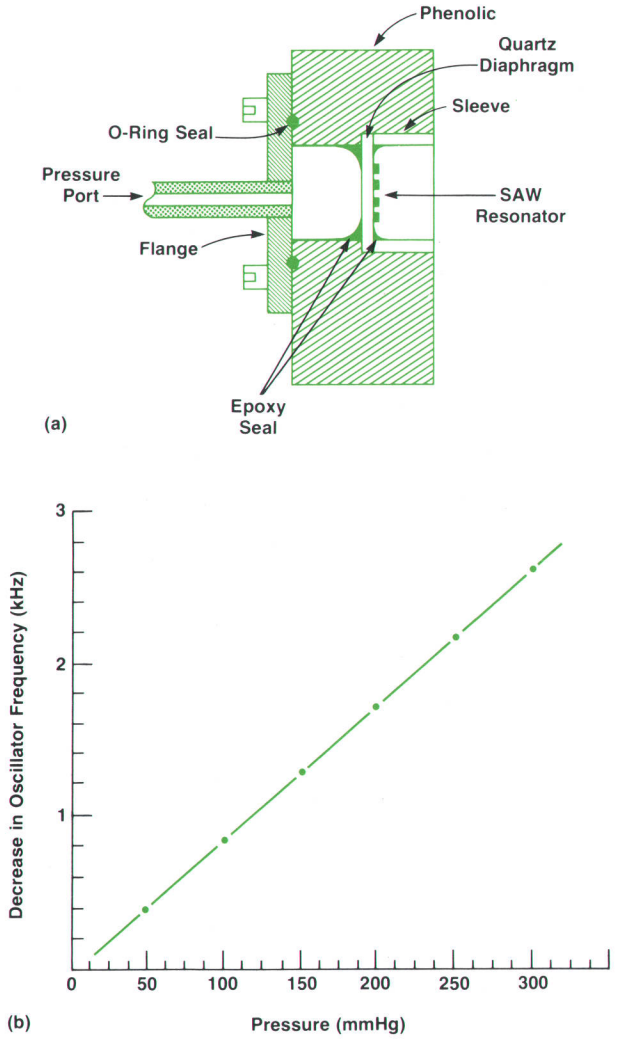

Fig. 6. *(a) Physical configuration of pressure sensor using a SAW resonator. (b) Change in resonant frequency versus pressure for sensor shown in (a).*

solely from quartz to eliminate the problem of matching the temperature coefficients of various parts of the sensor.

Sensors can also be made from the resonator configurations described on page 13.[3] An example of a pressure transducer is shown in Fig. 6, where the resonator is located in the middle of a diaphragm and the pressure is applied to the opposite face. The change in oscillator frequency is linear with pressure as shown by Fig. 6b.

J. Fleming Dias

Fleming Dias received the BE degree in civil engineering from the University of Poona, India, in 1954, the MSE degree (1957) in civil engineering and the BSE degree (1958) in electrical engineering from the University of Michigan, and the MS degree in electrophysics from DePaul University, Chicago, Illinois in 1970. He joined HP in 1972 with previous experience in stereo FM demodulators, SAW IF filters for TV receivers, and acousto-optic modulators. At HP he has worked on SAW oscillators for force sensors, the technology for the HP 1290 blood pressure transducer and the phased array transducer used in the HP 77020 Ultrasound Imaging System, and fiber-optic technology. He recently left HP to work on acoustic imaging systems. As an author or co-author Fleming has written thirteen papers and is named as the inventor or co-inventor on over 25 patents related to topics concerned with the various technologies he has worked on. He is a senior member of the IEEE and a native of Goa, India. Fleming and his wife live in Palo Alto, California and he enjoys photography, music, and travel when he is not experimenting in his home electronics laboratory.

Acknowledgments

The author gratefully acknowledges the technical assistance given by George Nelson and Henry Yoshida in processing the quartz substrates. René Cook and Dorothy Hollars were responsible for the intricate photolithography work and wire bonding of the IDTs. Al Benjaminson designed the wideband amplifiers and together with Ed Karrer provided many helpful ideas on sensor applications.

References:

1. J. F. Dias and H.E. Karrer, "Stress Effects in Acoustic Surface-Wave Circuits and Applications to Pressure and Force Transducers," 1974 IEEE International Solid-State Circuits Conference Proceedings, pp. 166-167.
2. A.L. Nalamwar and H. Epstein, "Strain Effects in SAW Devices," Proceedings of the IEEE, Vol. 64, no. 5, May 1976, pp. 613-615.
3. J.F. Dias, H.E. Karrer, J.A. Kusters, and C.A. Adams, "Frequency/Stress Sensitivity of SAW Resonators," Electronics Letters, Vol. 12, no. 22, October 28, 1976, pp. 580-582.

Proximity Effect Corrections by Means of Processing: Theory and Applications

HP's electron beam lithography system has been used to evaluate methods of reducing the unwanted effects of electron scattering.

by Paul Rissman and Michael P.C. Watts

IN ELECTRON BEAM LITHOGRAPHY, the proximity effect is the unwanted exposure of resist caused by electrons scattering in the resist layer and from the substrate. This leads to pattern features different from those designed. It is a major limitation to the fabrication of high-resolution integrated circuit devices by means of electron beam lithography. The proximity effect has been investigated by means of a computer model, and processing methods that can improve pattern fidelity have been explored. Significant reduction in the proximity effect can be achieved by two methods: the small-beam approach and multilayer resist techniques. Both of these methods have been tested experimentally on the HP electron beam lithography system described in these pages in May 1981.[1]

The cause of proximity effect may be seen in Fig. 1, which shows the calculated trajectories of 100 electrons incident at a point on a silicon surface coated with a layer of resist 0.4 μm thick.[2] The range of the scattered electrons is large; energy can be distributed as far as 6μm from the point being exposed. The way that this scattering affects the lithographic results is illustrated by Fig. 2, which shows modeling data for 0.4 μm of PMMA* electron-sensitive resist on silicon exposed by single scans of a 0.5-μm-diameter

*Polymethyl methacrylate

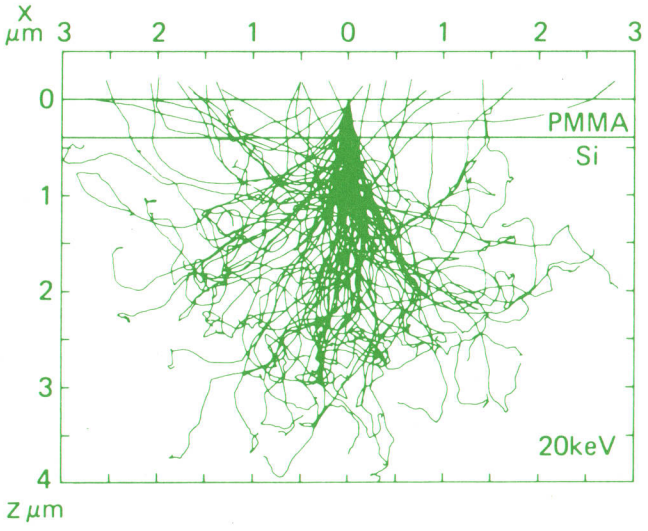

Fig. 1. *The calculated trajectories of 100 electrons with an energy of 20 keV incident on a 0.4-μm-thick PMMA resist layer on a silicon substrate (from Kyser and Murata[2]).*

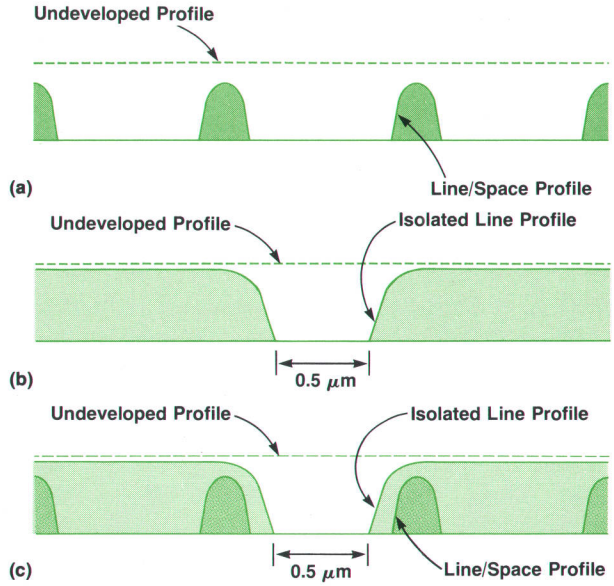

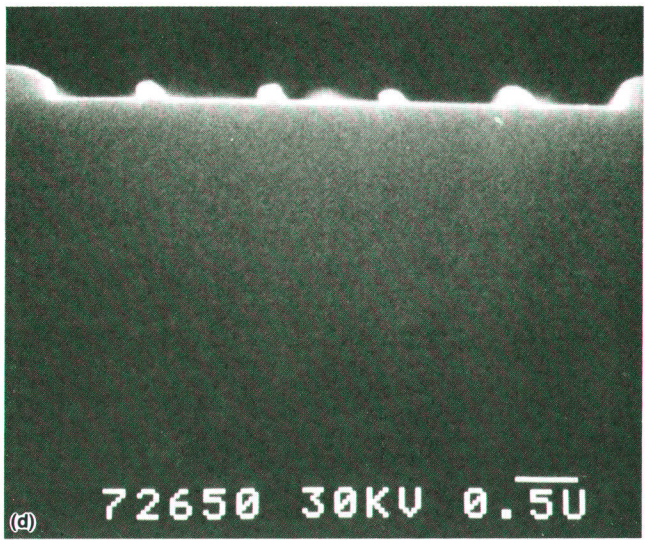

Fig. 2. *Proximity effect for lines exposed with a single scan of a 0.5-μm-diameter beam into a 0.4-μm-thick layer of PMMA resist on a silicon substrate. The pixel width is 0.5 μm. Shown are modeled profiles of the developed resist for (a) the central region of five 0.5-μm-wide lines with 0.5-μm-wide spacing and (b) an isolated 0.5-μm-wide line. (c) shows (a) and (b) superimposed for comparison. (d) SEM photograph of experimental result for five equal lines and spaces in PMMA.*

20-keV electron beam. Fig. 2a shows the result for the central region of a series of five 0.5-μm-wide lines and spaces (the lines are the exposed regions), and Fig. 2b shows the result for an isolated 0.5-μm-wide line. The width of the center line of the line-space combination is 50% larger than that of the isolated line. The resist wall angle is sloping, and there is considerable thinning of the resist in the unexposed region. Fig. 2d shows a scanning electron microscope (SEM) picture of several 0.5-μm lines and spaces exposed on the HP electron beam lithography system. The experimental and model profiles are in good agreement.

Various methods have been used to limit the proximity effect. The most widely used method involves preprocessing the input data and modifying the dose at exposure time. This method has been used with vector-scan electron beam systems.[3] A second method also involves preprocessing the input data; the exposure shapes are modified by the addition or subtraction of scans to achieve a uniform dose. This method has been applied to electron beam systems that are modified electron microscopes, where the smallest patterns are formed by many beam scans.[4]

In our work, other methods, which do not preprocess the input data, have been used to limit the proximity effect. Some of these techniques involve special resist processing, hence the term: proximity effect correction by processing. These processing techniques reduce proximity effect by minimizing the effect of backscattered electrons and reducing their number.

The model for electron beam exposure and development, which was written by Steve Eaton and Armand Neukermans, is described in the box on page 24. This model is an extremely useful tool for the process engineer to gain an understanding of the exposure and development of positive electron resist (i.e., exposed areas are removed when the resist is developed). Simulation parameters such as exposure dose and development time can be varied easily. Variables such as resist contrast or substrate material, which are not so readily adjusted experimentally, can be changed quickly to gain an understanding of their relationship to electron beam lithography performance.[5]

Modeling data can be used to improve the understanding of the process by plotting the resist profile as a function of development time. Fig. 3 illustrates this for a 0.5-μm line written with one, two, and four scans of an electron beam that has a Gaussian intensity profile along its diameter and beam diameters of 0.5, 0.25, and 0.125 μm, respectively (Fig. 4). The contours represent the line profile at 25-second development-time intervals. It can be seen that linewidth control is enhanced by writing lines with multiple beam scans. In addition, proximity effect is reduced by the use of multiple beam scans. However, there is a penalty paid in this approach because of the increased amount of data to be handled and the increased exposure time. For an increase by a factor n in the number of scans per critical dimension the beam must address n^2 additional pixels.

The use of a single scan for critical dimensions has distinct advantages in terms of increased throughput. There are disadvantages, however, most specifically the problem of lines written perpendicular to the raster-scan direction. As the HP electron beam system is presently configured, these lines consist of individual blankings of the beam. Thus they will appear as tangentially connected spots if the proximity effect is totally eliminated and the single-scan approach is used.

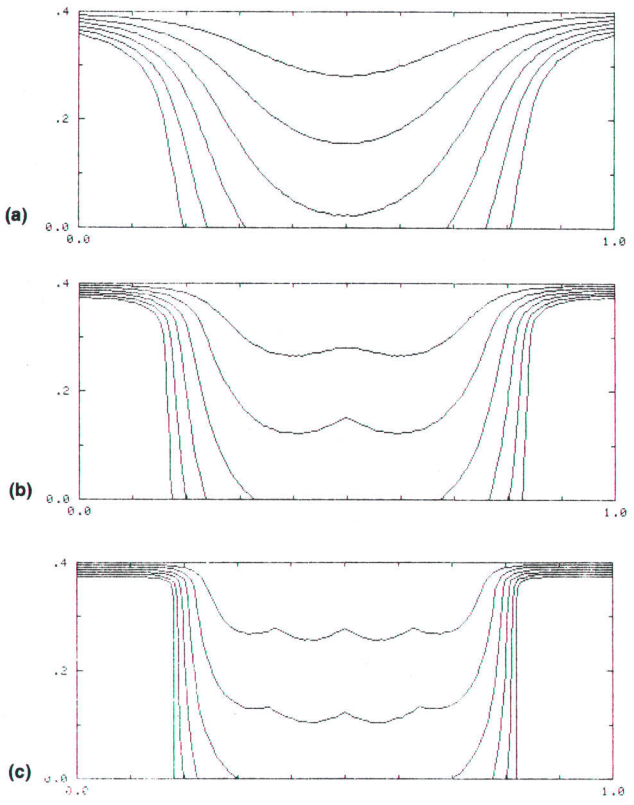

Fig. 3. *Modeling data for resist profiles at 25-second intervals during development for a 0.5-μm-wide isolated line exposed with (a) one scan of a 0.5-μm-diameter beam, (b) two adjacent scans of a 0.25-μm-diameter beam, and (c) four adjacent scans of a 0.125-μm-diameter beam.*

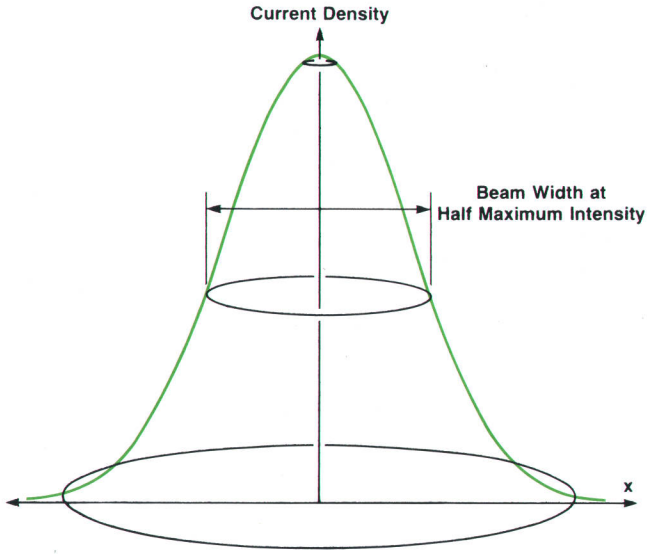

Fig. 4. *Gaussian electron beam current density profile showing how beam diameter is defined.*

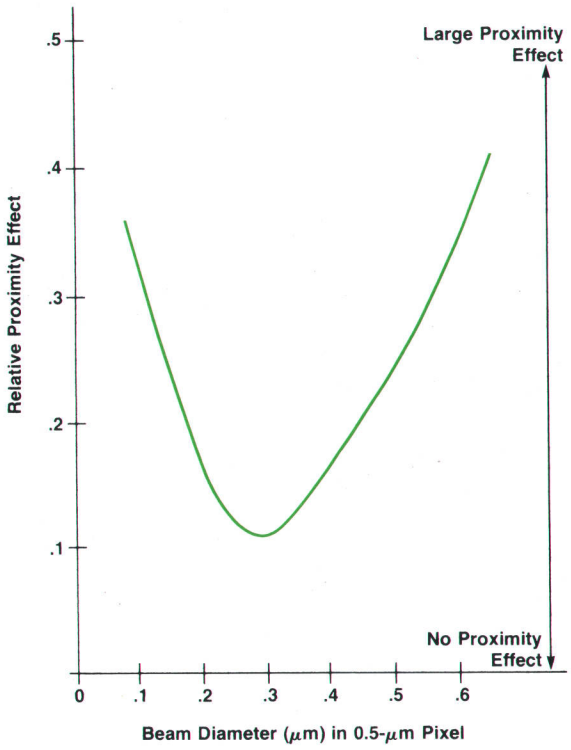

Fig. 5. *Variation of proximity effect as the beam diameter is varied in a 0.5-μm pixel.*

Small-Beam Approach

In conventional electron beam lithography, the beam diameter (width at half maximum intensity) is chosen to be the same as the pixel width (i.e., a 0.5-μm beam is used with a 0.5-μm-wide pixel). The modeling indicates, however, that this may not be the optimum approach. For a 0.5-μm-wide pixel, a minimum proximity effect can be found at a beam diameter of about 0.3μm (see Fig. 5). This minimum can be explained by considering the energy delivered into the pixel and noting that at the 0.5-μm beam diameter, the energy is not maximized.[6,7]

The reduction in the proximity effect can be seen in Fig. 6, which shows modeling data similar to that shown in Fig. 2, but for a 0.3-μm-diameter beam. The linewidth for the line/space combination is closer to that for the isolated line, indicating a reduction of the proximity effect. Also, the resist profiles have steeper slopes and the resist remaining in the unexposed areas is sufficient to protect the underlying layer during pattern etching. Linewidth control is improved by a factor of four over the result for a 0.5-μm beam. Experimental results confirm the predictions of the model. Fig. 6b is an SEM photograph of 0.5-μm-wide lines and spaces exposed with a 0.28-μm-diameter electron beam. The profiles are much improved over those obtained with a 0.5-μm beam (Fig. 2).

The small-beam approach reduces the proximity effect and makes greater linewidth control possible, but it also reduces machine throughput because the reduction in beam diameter leads to a smaller beam current (beam current density is approximately constant).

Multilayer Resist

Multilayer resist systems are a useful method to extend the range of optical lithography.[8,9,10] A thick bottom layer allows good step coverage and provides a means of smoothing the substrate surface. Multilayering can also limit the proximity effect by placing the electron-sensitive layer outside the range of the electrons backscattering from the substrate surface. Modeling data indicates that, as the thickness of the bottom absorbing layer is increased, the proximity effect is reduced. For bottom layers thicker than 2.5 μm no further reduction is obtained because backscattering from the bottom layer then becomes the significant contribution to proximity effect.

Fig. 7a shows modeling data for a 3-μm-thick polymer absorbing layer. The improvement over the data displayed in Fig. 2 is evident. The linewidths are nearly the same and almost all of the initial resist thickness remains in the unexposed region. The resist wall slope reflects the Gaussian intensity profile of the 0.5-μm diameter electron beam used for exposure. Further improvement can be obtained by using a small beam approach with a multilayer structure. The modeling data in Fig. 7b shows the result for a 0.3-μm-

(continued on page 25)

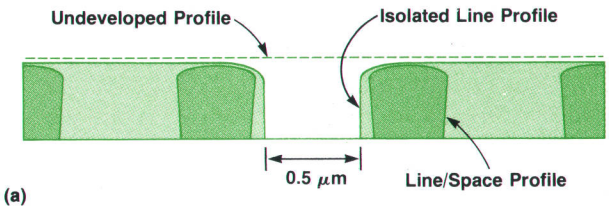

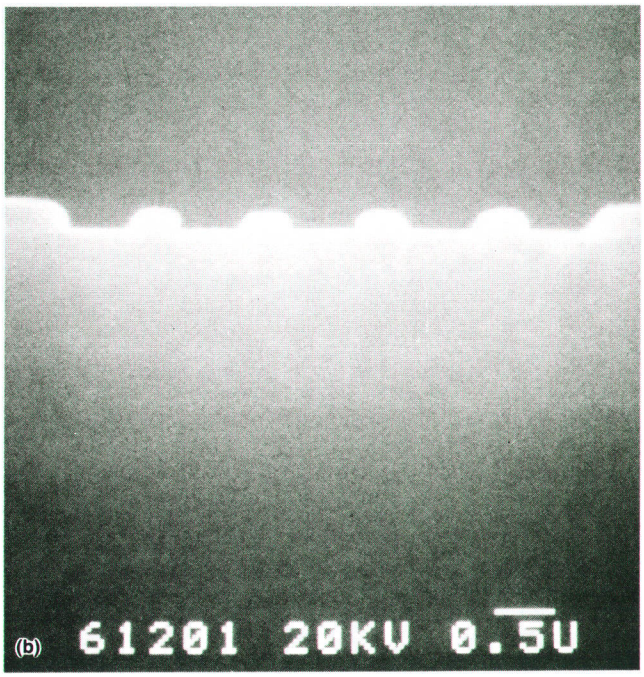

Fig. 6. *Proximity effect reduction in lines exposed under the same conditions as for Fig. 2 except that the beam diameter is reduced to 0.3 μm. (a) Superimposed for comparison are modeled profiles of the developed resist for the central region of five 0.5-μm-wide lines with 0.5-μm-wide spacing and an isolated 0.5-μ-wide line. (b) SEM photograph of a cross section through five equal lines and spaces in PMMA.*

Monte Carlo Simulations for Electron Beam Exposures

by Armand P. Neukermans and Steven G. Eaton

When energetic electrons (20 keV) interact with matter they penetrate and scatter quite appreciably on a microscopic scale. For infinitely thick targets, this behavior can be described analytically in terms of forward and backward scattered distributions. This analytical approach becomes difficult when multiple-layered structures such as resists on silicon must be studied.

A few years ago a Monte Carlo method was developed, initially to describe backscattering from alloys.[1] Later the technique was carried over to proximity problems in electron lithography. As the name Monte Carlo implies, dice, or more approporiately random numbers, are used to simulate the behavior of electrons statistically.

Suppose, for example, that an electron can cause one of three events: A with a probability of 20% , B with a probability of 50% , or C with 30% probability. We generate a random number α ($0 \leq \alpha \leq 1$) and decide that A happens for $0 \leq \alpha < 0.2$, B occurs for $0.2 \leq \alpha < 0.7$, and C occurs for $0.7 \leq \alpha \leq 1$. If the random number is truly random, over a large number of trials the three events will occur the correct number of times. In a very similar way, we can describe processes that have continuous probability densities. Consider, for example, a fictitious electron scattering process, as illustrated in Fig. 1a. All scattering angles are possible, but not equally probable. We generate from this graph a cumulative distribution by integration and normalization (Fig. 1b). Each random number α is made to correspond to a scattering angle as indicated. Again, over many events, scattering according to the pattern of Fig. 1a will occur. This basic procedure with some variants allows us to simulate very complex problems, provided we know the probabilities of all possible events and repeat the process enough times to obtain statistically meaningful data.

Consider an electron approaching a resist layer on silicon under normal incidence. Since we know its energy, we know its mean free path, the rate at which it is losing energy (the Bethe energy loss formula[2]) and its probability of interaction with each of the atoms of the resist (C, H, O, Cl,...). It travels in a straight line until it collides with one of the resist atoms, whereupon it scatters elastically (screened Rutherford scattering[3]). Its direction is now changed, its energy is slightly different from before, and the energy loss rate and interaction cross-section are slightly modified. This process is continued until the energy of the incoming electron is spent, which may require several hundred collisions. Its position is monitored, since it may enter the silicon where different scattering conditions exist, or turn around (backscatter) and leave the resist, in which case the calculation is terminated.

The process is repeated over and over again with other electrons under identical impact conditions. The resist space under the impact point is divided into a number of toroidal boxes. As successive electrons traverse a box the energy lost by each electron in that box is registered and accumulated.

After twenty to thirty thousand electron impacts the dissipated energy distribution, as given by the content of these boxes, becomes quite smooth. We now have obtained the three-dimensional point-spread function of the energy distribution around the impact point. This may be convolved with the beam distribution (usually Gaussian) and beam strength to obtain the energy distribution under a real beam. Once this exposure data is known for the resist, it can be coupled with a development model, which describes how the resist develops as a function of exposure. The Berkeley SAMPLE program[4] was modified to do this.

The original program was written in ALGOL on an HP 1000 Computer. Simulating enough electrons required several days,

(continued on next page)

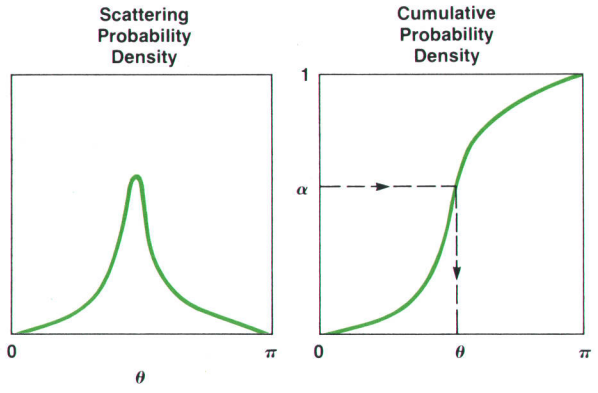

Fig. 1. *If scattering angles occur randomly according to the probability density (a), their cumulative distribution is (b), and each angle can be made to correspond to a random number α as indicated. In computer simulations with a random number generator, scattering according to (a) will be simulated.*

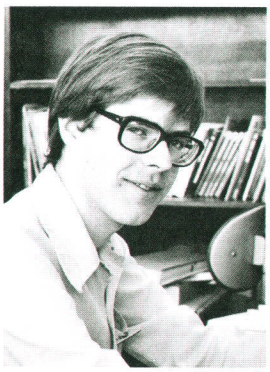

Steven G. Eaton

Steven Eaton worked on the electron beam exposure simulation program in 1979 while he was still a student. He joined HP Laboratories in 1980 after receiving his BS degree in engineering and his MS degree in electrical engineering from California Institute of Technology. He's now working on x-ray lithography technology development. Steven's home town is Salina, Kansas, and he now lives in Palo Alto, California. Bicycling heads his list of interests.

Armand P. Neukermans

Armand Neukermans is manager of HP Laboratories' x-ray lithography project. Born in Okegem, Belgium, he received his BSME and BSEE degrees from Louvain University in 1962, did engineering work for the next six years, and then returned to school and received his MSEE degree from Arizona State University in 1967 and his PhD in applied physics from Stanford University in 1970. After three years of xerographic physics research, he joined HP Laboratories in 1973. Among his contributions are a cesium iodide medical x-ray imaging screen and an electron capture detector for gas chromatography. His work has resulted in nine patents and 12 papers. He's member of IEEE. Armand is married, has four children, lives in Palo Alto, California, teaches religious education, and enjoys jogging and swimming.

which was prohibitively long. Steven Eaton rewrote the program in assembly language and FORTRAN and improved it to the point where a point-spread function is now obtained in one to two hours. Beam sizes or scan rates are then convolved very rapidly and the resultant etch patterns displayed. This makes it a very powerful tool for setting up resist experiments and understanding resist patterns in electron beam lithography.

References

1. K. Murata, T. Matsukawa, and R. Shimizu, "Monte Carlo Calculations on Electron Scattering in a Solid Target," Japanese Journal of Applied Physics, Vol. 1, p. 678, 1971.
2. H.A. Bethe, Handbuch der Physik, Springer-Verlag, Vol. 24, p. 519, 1933.
3. G. Wentzel, Z. Phys., Vol. 40, p. 590, 1927.
4. S.N. Nandgaonkar, "Design of a Simulator Program (SAMPLE) for IC Fabrication," University of California at Berkeley ERL Report M79/16, June 1978.

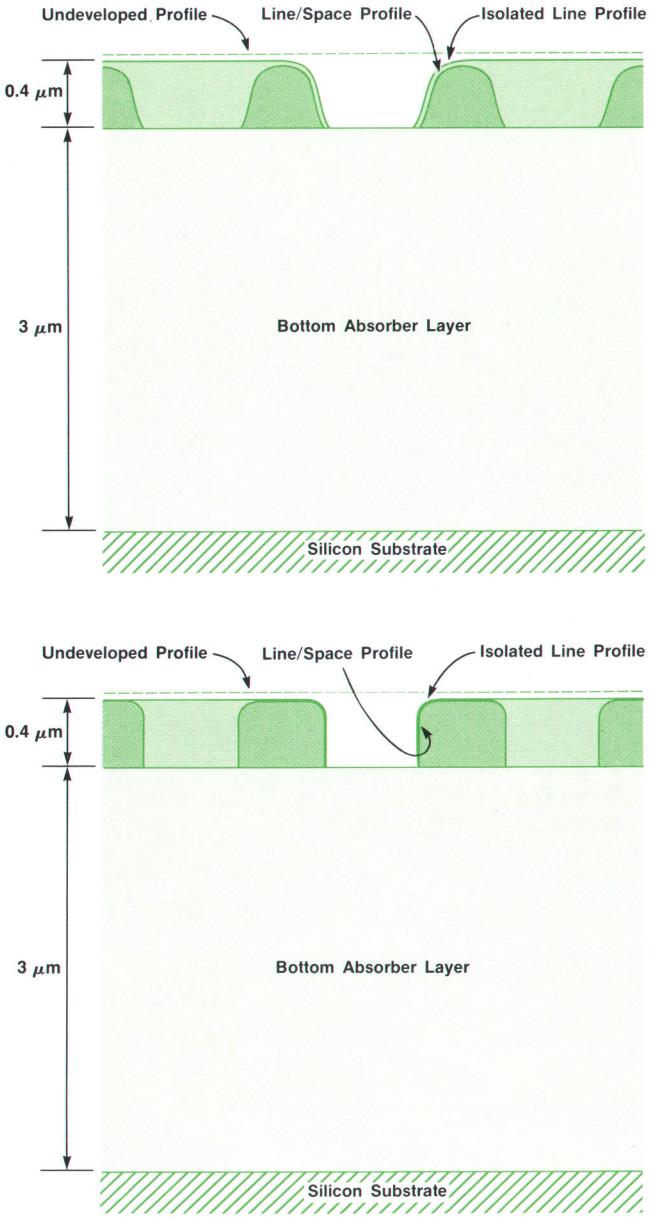

Fig. 7. *Proximity effect reduction for lines exposed under the same conditions as for Figs. 2 and 4 except that a 3-μm-thick absorbing polymer layer is used under the 0.4-μm-thick resist layer. Shown are modeled profiles of the developed resist for the central region of five 0.5-μm-wide lines with 0.5-μm-wide spacing and an isolated 0.5-μm-wide line. (a) Beam diameter 0.5 μm. (b) Beam diameter 0.3 μm.*

diameter beam. The experimental verification of the multilayer method is shown in Fig. 8. The SEM photos show the center lines of single-scanned 0.5-μm-wide lines as the spacing between the lines is varied. Shown are spacings of 0.5μm, 1 μm, 1.5 μm, 2.0 μm and 4 μm, where lines with 4-μm spacing can be considered as a series of isolated lines. There is little linewidth variation; this can be attributed to the 3-μm-thick absorber layer used.

A problem of the multilayer technique is how to transfer the well-defined features in the thin top resist layer to the thick bottom layer. In the trilevel process, the pattern is transferred from the resist image layer to a thin interlayer, which acts as a mask for oxygen reactive-ion etching of the thick bottom layer.[8] The transfer method is anisotropic, and aspect ratios as high as 5:1 (depth:linewidth) can be achieved. Many materials have been used for the intermediate and base layers. At HP, a silicon interlayer process was developed for the multilevel resist systems.[11] Silicon is attractive as an interlayer because it is a noncontaminant to integrated circuit processing, it is resistant to the oxygen plasma etch, it will not charge during electron beam exposure, and it can be easily deposited by evaporation or sputtering techniques. Typically, Hunt's HPR resist was used as the bottom layer although PMMA can be used if undercutting of this layer can be tolerated. Fig 9 shows an isolation level for a RAM device patterned in the bottom layer of the trilevel structure. For this experiment, PGMA negative electron beam resist was used with a silicon interlayer and 3 μm of HPR as the bottom layer. The smallest critical dimensions are 1 μm.

The elimination of backscattering by the use of multilayer resist systems has raised an additional concern for direct

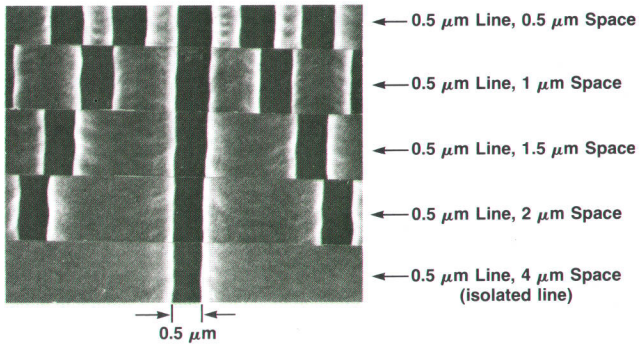

Fig. 8. *Proximity effect reduction using multilayer technique. The SEM photographs show the actual widths of 0.5-μm-wide lines as the spacing between the lines is varied from 0.5 μm to 1.0 μm, 1.5 μm, 2.0 μm, and 4.0 μm. The multilayer structure consists of the patterned layer (0.4-μm-thick layer of PMMA resist), the transfer layer (0.07-μm-thick silicon film), and the absorber layer (3-μm-thick layer of Hunt HPR resist). The beam diameter in this experiment was equal to the pixel width.*

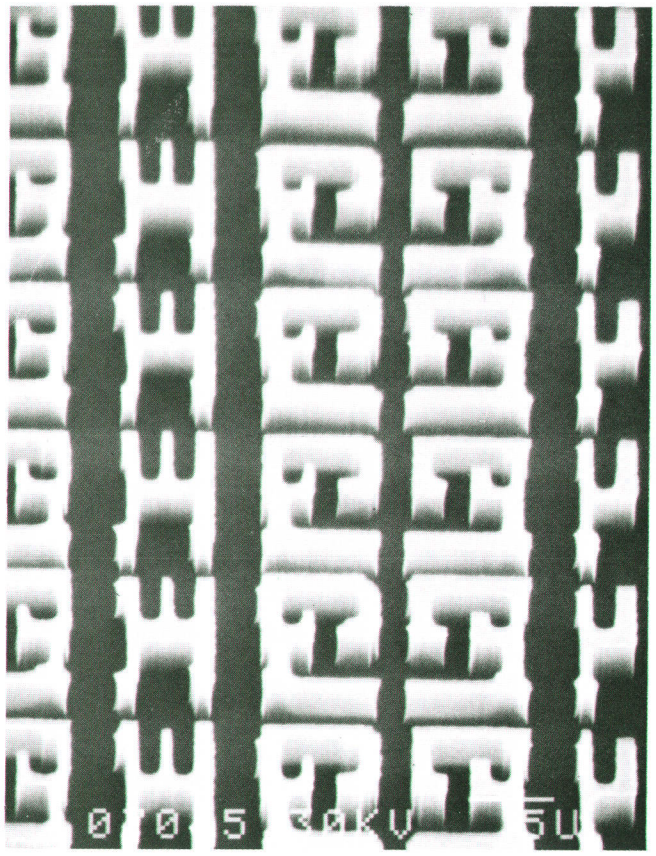

Fig. 9. *This is a scanning electron micrograph of the isolation level for a portion of a random-access memory (RAM) patterned in the bottom layer of a trilevel resist structure. The top layer was exposed in the HP electron beam lithography system. The multilayer process reduces proximity effect and gives high-aspect-ratio lines ideal for masking dry etch processes. The smallest critical dimensions shown are 1 μm.*

writing. Since the electron beam itself is used as a probe to find fiducial marks on the wafer surface, the thick absorber layer could obscure the fiducial signal. Experiments, however, prove that this is not the case. As shown in Fig. 10, thick resist degrades the fiducial mark signal from that obtained with a single resist layer, but the machine is able to locate the fiducial mark centers.

Two other techniques of pattern transfer involve two-layer methods. The first is the patterning of the bottom layer by deep-ultraviolet (UV) radiation.[9] If the electron-beam-sensitive top layer absorbs UV, a flood UV exposure can be used for image transfer.

The second technique involves using a bottom absorber layer that is electron-beam-sensitive. If the developer for the top layer leaves the bottom layer unchanged and vice versa, optimum liftoff* structures can be produced.[10] While this method is limited in its application to producing high-aspect-ratio resist structures, it does provide a means to reduce the proximity effect in several special applications (0.3-μm-wide lines and spaces have been fabricated for surface acoustic wave devices). This method has another distinct advantage. Because the bottom layer is not affected by the top-layer developer, a pinhole in the top layer will not be transferred to the metal structure produced by liftoff. Consequently, extremely thin and hence high-resolution image layers can be used.

An example of model output and experimental resist profiles for liftoff structures with 0.5-μm lines and spaces is shown in Fig. 11. These structures have been used to produce surface acoustic wave devices with critical dimensions of 0.5 μm and 0.3 μm that operate at 1.6 GHz and 2.6 GHz, respectively.[12]

Acknowledgments

Understanding of the proximity effect was greatly enhanced by means of Armand Neukermans' and Steve Eaton's computer model. The resist reactive-ion etch work presented here is a joint project of one of the authors (PR) with Jim Kruger and Mark Chang of HP's Physical Electronics Lab (PEL). The authors would like to thank their colleagues, Hsia Choong, Marsha Long, Rich Meriales, Dick

*Liftoff is a process in which a layer, typically metal, is desposited on a wafer and the unwanted portions are "lifted off" by dissolving the resist under them. Application of the technique requires the production of the mushroom-like resist structures shown in Fig. 11. The undercut structure allows solvent to get in and dissolve the stem of the mushroom, thereby removing anything deposited on the top of the mushroom. The material deposited between the mushrooms is not removed.

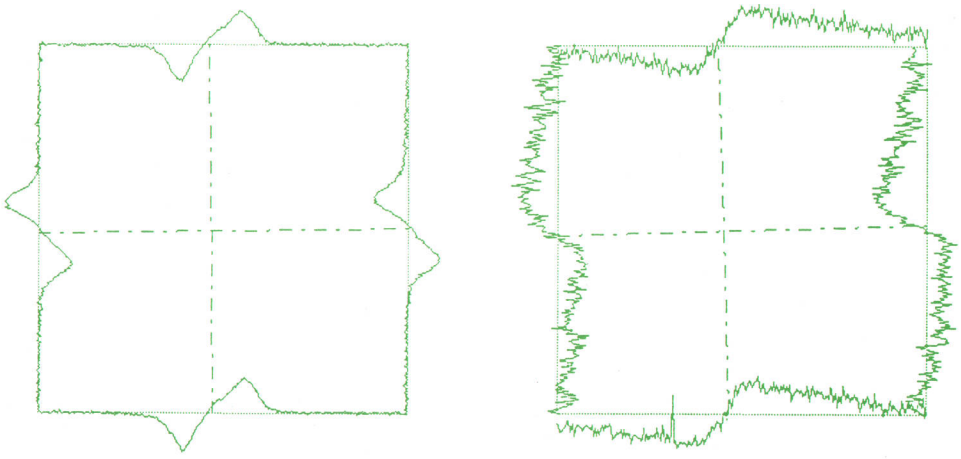

(a) Signal on Single-Layer Resist

(b) Signal on Multilayer Resist with 3-μm Bottom Layer

Fig. 10. *Photomultiplier output data from electron beam scans across four arms of a fiducial mark covered with (a) a thin resist coating and (b) a multilayer resist structure. The centers of the arms of the mark are indicated by the broken lines. The signal from the mark covered with thick resist is degraded, but accurate alignment is still possible.*

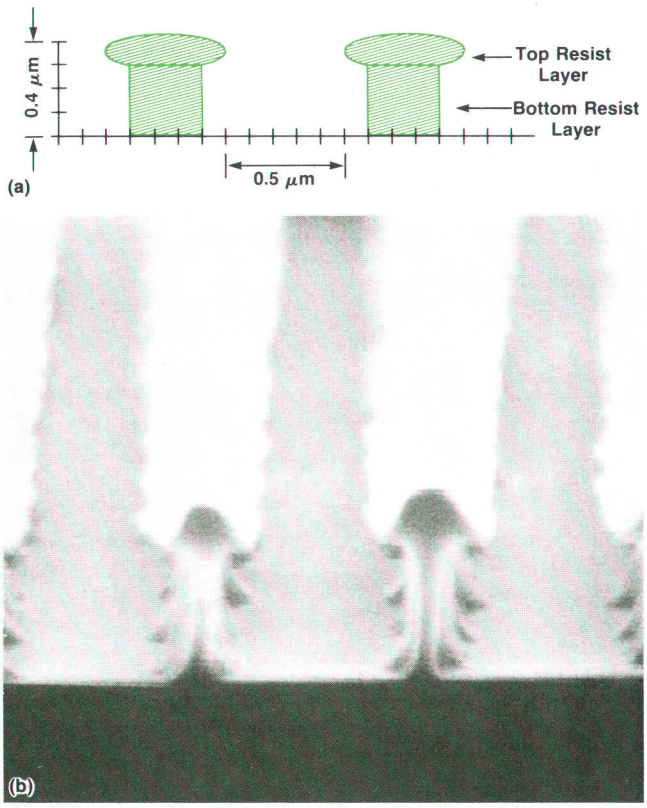

Fig. 11. *Mushroom-shaped liftoff structures can be generated by using a two-layer process where the developer for each layer does not affect the other layer. The bottom layer is overdeveloped, creating the undercut profile modeled in (a) for 0.5-μm-wide lines and spaces using a 0.3-μm-thick bottom layer and a 0.1-μm-thick top layer. (b) SEM photograph of the experimental result.*

Moung, Steve Muto, Judith Seeger, and Jen-Te Wang for their help and encouragement. Finally, the authors are indebted to Frank Ura (PEL) and Fredrick Kahn of HP's Solid State Lab (SSL) for providing an environment that has made this research possible.

References

1. J.C. Eidson, W.C. Haase, and R.K. Scudder, "A Precision High-Speed Electron Beam Lithography System," Hewlett-Packard Journal, May 1981.
2. D. Kyser and K. Murata, "Monte Carlo Simulation of Electron Beam Scattering and Energy Loss in Thin Films on Thick Substrates," Proceedings of the Sixth International Conference on Electron and Ion Beam Science and Technology, Electrochemical Society, 1974, pp. 205-223.
3. M. Parikh, "Corrections to Proximity Effects in Electron Beam Lithography," Journal of Applied Physics, Vol. 50, 1979, pp. 4371-4387.
4. C. Youngman and N. Wittels, "Proximity Effect Correction in Vector-Scan Electron-Beam Lithography," SPIE Developments in Microlithography III, 135, (1978), pp. 54-58.
5. P. Rissman, "Studies of Proximity Effect by Computer Modeling of Electron Beam Exposure and Development," unpublished internal HP report, April 1980.
6. J.S. Greenich, "Impact of Electron Scattering on Linewidth Control," Journal of Vacuum Science and Technology, Vol. 16, 1979, pp. 1749-1753.
7. P. Rissman and M. Watts, "Optimization of Beam Diameter for Proximity Effect Reduction," in preparation.
8. J. Moran and D. Maydan, "High Resolution, Steep Profile Resist Patterns," Bell System Technical Journal, Vol. 58, 1979, p. 1027.
9. B. Lin, "Portable Conformable Mask - a Hybrid Near-Ultraviolet and Deep Ultraviolet Patterning Technique," SPIE Developments in Semiconductor Microlithography IV, 174, (1974), pp. 114-121.
10. I. Haller, R. Feder, M. Hatzakis, and E. Spiller, "Copolymers of Methymethacrylate and Methacrylic Acid and their Metal Salts as Radiation Sensitive Resists," Journal of the Electrochemical Society, Vol. 126, 1979, p. 154.
11. J. Kruger, P. Rissman, and M. Chang, "Silicon Transfer Layer for Multi-layer Resist System," Proceedings of the 16th Symposium on Electron, Ion and Photon Beam Technology, May 1981, Dallas, Texas (to be published).
12. P.S. Cross, P. Rissman, and W.R. Shreve, "Microwave SAW Resonators Fabricated with Direct-Writing Electron-Beam Lithography," Proceedings of the 1980 Ultrasonics Symposium, pp. 158-163.

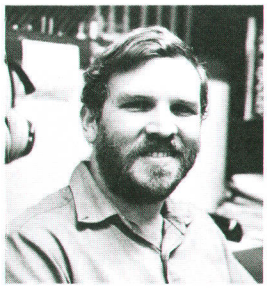

Paul Rissman
Paul Rissman has been working on electron beam processing since he joined HP in 1979. A graduate of the University of Wisconsin at Madison, he received his BS and MS degrees in electrical engineering in 1971. Paul has extensive experience in electron lithography and other areas of research. He has authored sixteen papers and is a member of the American Vacuum Society.

Michael P.C. Watts
Michael Watts joined HP in 1979. His work has included the study of new resist materials for electron beam and x-ray lithography. He received the BSc and PhD degrees in polymer science and technology from the University of Manchester Institute of Science and Technology in 1974 and 1977 respectively, did postdoctoral research at the University of Massachusetts, and has authored several papers on multiblock polymers, ultra-high-modulus polyethylene, and positive resist characterization. He is a member of the American Chemical Society.

HEWLETT-PACKARD JOURNAL

Volume 32 January 1981 through December 1981

Index

Hewlett-Packard Company, 3000 Hanover Street, Palo Alto, California 94304 U.S.A.
Hewlett-Packard Central Mailing Department, Van Heuven Goedhartlaan 121, 1181 KK Amstelveen, The Netherlands
Hewlett-Packard (Canada) Ltd., 6877 Goreway Drive, Mississauga, Ontario L4V 1M8 Canada
Yokogawa-Hewlett-Packard Ltd., Suginami-ku, Tokyo 168 Japan

PART 1: Chronological Index

PART 2: Subject Index

PART 3: Model Number Index

PART 4: Author Index

F

Federman, Nancy C. Apr. 1981
Flower, Terry L. Nov. 1981
Frankel, Andrea K. Nov. 1981

G

Gaullier, Francois Jan. 1981
Gilbert, Robert A. July 1981
Graham, Gordon C. Mar. 1981
Griffin, Daniel J. June 1981
Groves, Timothy R. May 1981
Gyma, Dennis W. Aug. 1981

H

Haase, Wayne C. May 1981
Hamilton, Bruce May 1981
Hanson, Fred L. June 1981
Hardage, P. Kent June 1981
Haselby, Robert D. Nov. 1981
Hassun, Roland Feb. 1981
Haugh, Samuel R. Nov. 1981
Haydamack, William J. June 1981
Heger, Thomas J. July 1981
Hennessee, Larry W. Nov. 1981
Hester, Richard L. July 1981
Heyl, Lawrence E. July 1981
Hsu, Tsen-gong Jim May 1981
Hyde, John W. Aug. 1981

I

Ishak, Waguih S. Dec. 1981
Ives, Fred H. Feb. 1981

J

Jones, Lawrence T. Apr. 1981
Jones, Vincent C. July 1981

K

Kaplan, Ronald J. Nov. 1981
Karrer, H. Edward Dec. 1981
Kelly, John May 1981
Khalily, Ebrahim June 1981
Kinsell, David A. Jan. 1981
Koerper, Steven J. Oct. 1981
Kovalick, Albert W. Feb. 1981
Krieger, John J. Sept. 1981
Kuo, Huei Pei May 1981
Kurtz, Barry D. Apr. 1981
Kusters, John A. Mar. 1981

L

LaBarre, Lawrence Oct. 1981
Laing, Virgil L. July 1981
Lee, Howard F. May 1981
Leonard, Mark G. Oct. 1981
Lewis, Robert B. May 1981
Li, Victor Aug. 1981
Lindberg, Earl E. May 1981
Lo, Clement C. Oct. 1981
Lubin, Donald L. Jan. 1981
Lynch, George W. Nov. 1981

M

Martini, Neal J. Nov. 1981
Mason, Martin K. Oct. 1981
Mathiesen, Donald W. Feb. 1981
McCalla, William J. June 1981
Merja, Charles L. May 1981
Merrick, Edwin B. Sept. 1981
Mierzwinski, Marek E. Dec. 1981
Mostafa, Hatem E. Nov. 1981
Myers, Richard Aug. 1981
Myers, Robert L. Aug. 1981

N

Narimatsu, Yoh Sept. 1981
Negrete, Marco June 1981
Neukermans, Armand P. Dec. 1981

O

Osborne, Ian F. May 1981
Overton, Mark A. Nov. 1981
Owen, Geraint May 1981

P

Packard, David June 1981
Parker, Russell A. Sept. 1981
Patterson, Marvin L. Nov. 1981
Peck, Robert D. Aug. 1981
Perach, David J. Nov. 1981
Platt, David L. Feb. 1981

Q

R

Redding, Patricia A. July 1981
Ressmeyer, James J. Apr. 1981
Revere, Thomas L., III Jan. 1981
Richard, Steven H. Jan. 1981
Richardson, John W. Feb. 1981
Rissman, Paul Dec. 1981
Roland, W. Vincent Aug. 1981
Roy, Jean-Claude Mar. 1981

S

Scampini, Steven A. Oct. 1981
Schaper, Dale W. Nov. 1981
Scheffer, Louis K. June 1981
Scherer, Dieter Feb. 1981
Schudy, Robert B. May 1981
Schwartz, Daniel R. Aug. 1981
Scudder, Ronald K. May 1981
Seipel, Winfried Aug. 1981
Shimizu, Takeo Sept. 1981
Shreve, William R. Dec. 1981
Smith, Richard B. Nov. 1981
Solomon, Rodney J. Sept. 1981
Son, Myungsae Nov. 1981
Staas, Gary C. Mar. 1981
Stavely, Donald J. Jan. 1981
Steiner, Robert M. Apr. 1981
Steinmetz, James H. Mar. 1981
Stewart, Lowell J. Nov. 1981
Sukumar, Srinivas Mar. 1981
Sweetser, David J. July 1981

T

Terrien, Mark E. Dec. 1981
Tiefert, Karl H. Aug. 1981
Tsang, Dah Wen Aug. 1981
Townsend, Robert S. Nov. 1981
Tucker, Michael G. June 1981
Tyler, Charles E. Oct. 1981

U

Uebbing, John J. Jan. 1981
Oct. 1981
Ura, Frank May 1981

V

W

Watts, Kenneth F. July 1981
Watts, Michael P.C. Dec. 1981
Weaver, Edward G., Jr. Jan. 1981
Wiese, John D. Mar. 1981
Wilson, Robert L. Mar. 1981
Winston, Loretta E. Apr. 1981
Wolpert, David L. July 1981

X

Y

Yagi, Kanuyaki Sept. 1981
Younge, Robert G. Oct. 1981

Z

Zimmer, Donald, Jr. Mar. 1981

Hewlett-Packard Company, 3000 Hanover Street, Palo Alto, California 94304

Bulk Rate
U.S. Postage
Paid
Hewlett-Packard
Company

HEWLETT-PACKARD JOURNAL

DECEMBER 1981 Volume 32 • Number 12
Technical Information from the Laboratories of Hewlett-Packard Company
Hewlett-Packard Company, 3000 Hanover Street
Palo Alto, California 94304 U.S.A.
Hewlett-Packard Central Mailing Department
Van Heuven Goedhartlaan 121
1181 KK Amstelveen, The Netherlands
Yokogawa-Hewlett-Packard Ltd., Suginami-Ku Tokyo 168 Japan
Hewlett-Packard (Canada) Ltd.
6877 Goreway Drive, Mississauga, Ontario L4V 1M8 Canada